LBL-9308 c.2

Lawrence Berkeley Laboratory

UNIVERSITY OF CALIFORNIA, BERKELEY, CA

Materials & Molecular Research Division

THE EFFECT OF COAL CHAR ON THE CORROSION OF 304 SS

Thomas Friedrich Wilhelm Foerster
(M. S. thesis)

RECEIVED
LAWRENCE
BERKELEY LABORATORY

JUL 23 1979

LIBRARY AND
DOCUMENTS SECTION

June 1979

TWO-WEEK LOAN COPY

This is a Library Circulating Copy
which may be borrowed for two weeks.
For a personal retention copy, call
Tech. Info. Division, Ext. 6782

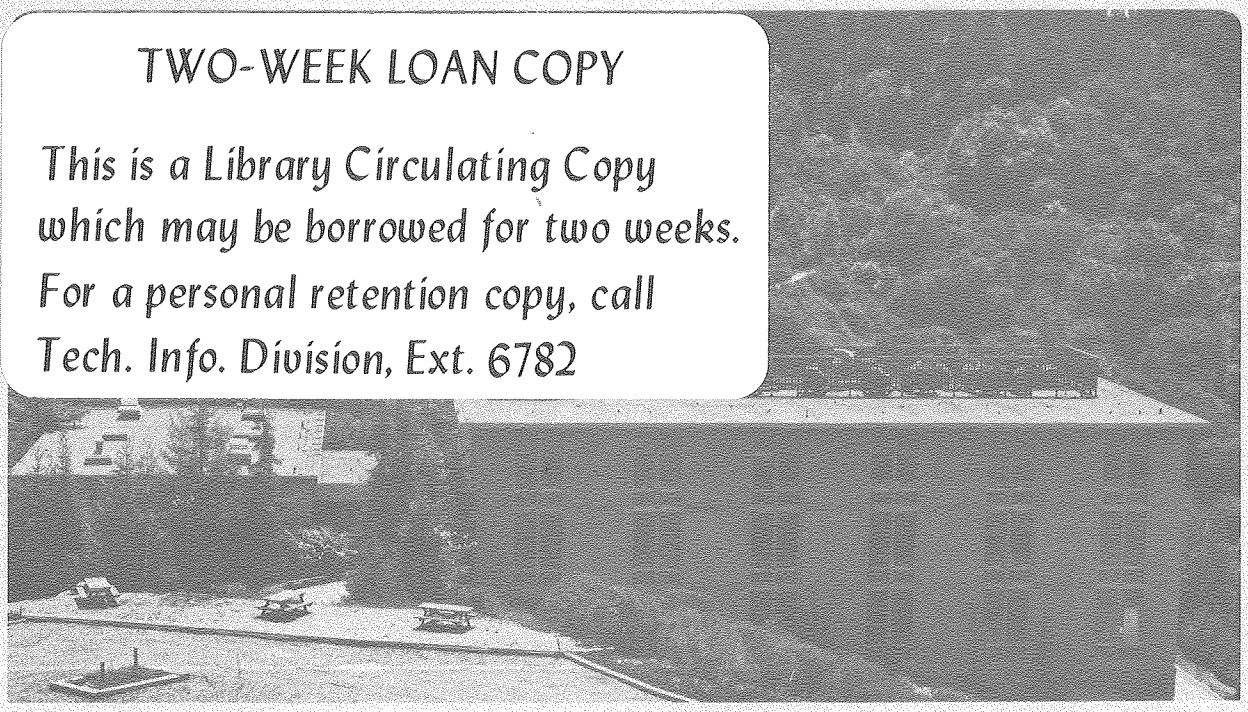

LBL-9308 c.2

Prepared for the U. S. Department of Energy
under Contract W-7405-ENG-48

DISCLAIMER

This document was prepared as an account of work sponsored by the United States Government. While this document is believed to contain correct information, neither the United States Government nor any agency thereof, nor the Regents of the University of California, nor any of their employees, makes any warranty, express or implied, or assumes any legal responsibility for the accuracy, completeness, or usefulness of any information, apparatus, product, or process disclosed, or represents that its use would not infringe privately owned rights. Reference herein to any specific commercial product, process, or service by its trade name, trademark, manufacturer, or otherwise, does not necessarily constitute or imply its endorsement, recommendation, or favoring by the United States Government or any agency thereof, or the Regents of the University of California. The views and opinions of authors expressed herein do not necessarily state or reflect those of the United States Government or any agency thereof or the Regents of the University of California.

ABSTRACT

It is demonstrated that a layer of coal char covering a metal surface affects the sulfur and oxygen partial pressures at the metal surface and thus the rate and extent of corrosion. Experiments demonstrating the effect of char composition and depth and bulk gas composition and flow rate on the rate of sulfidation are carried out. A simple theoretical model, which predicts the concentration profiles and fluxes of the gaseous species in the char, is solved.

Since coal char contains carbon, the equilibrium oxygen partial pressure is less than 10^{-18} atm. This low oxygen partial pressure prevents the formation of protective oxide scales and, in some cases, leads to the formation of external sulfide scales.

The effect of the layer of char on the sulfur partial pressure at the metal surface depends on the composition of the char. If the char contains a large amount of sulfur-rich volatiles, the sulfur partial pressure of the gas in the char and the extent of sulfidation depend on the composition of the volatiles. If the char contains significant amounts of inorganic ash, the sulfur partial pressure of gas in contact with the char is determined by the equilibria of the various reactions between hydrogen sulfide and ash. For both types of char described above, the pattern and extent of corrosion of samples exposed for short times are essentially independent of the composition of the bulk gas and the thickness of the char layer. If the char does not contain large amounts of ash or all of the ash has reacted, the sulfur partial pressure at the metal surface is determined by the diffusion of hydrogen sulfide through the char layer. In this case the rate of sulfidation is inversely proportional to the thickness of the char

layer and roughly directly proportional to the concentration of hydrogen sulfide in the bulk gas.

TABLE OF CONTENTS

	Page
Abstract	i
Chapter 1: Introduction	1
A. Thermodynamics of Sulfidation and Oxidation	9
B. Mechanism and Kinetics of Oxidation/Sulfidation	12
C. Previous Work on the Effect of Char on Corrosion	13
D. Objectives	14
Chapter 2: Model of Mass Transfer through Coal Char	18
A. Assumptions	18
B. Governing Equations	18
C. Physical Properties	23
D. Boundary Conditions	25
E. Solution of Governing Equations	25
F. Thermodynamics of Char-Gas Reactions	28
G. Results for Steady State	33
H. Transient Results	38
Chapter 3: Experiments	44
A. Apparatus	44
B. Experimental Procedure	47
C. Experiments	47
D. Corrosion in Sulfur-Free Bulk Gases	50
E. Corrosion in Sulfur Containing Bulk Gases	60
Chapter 4: Discussion	79
A. Effect of Coal Char on the Oxygen Partial Pressure	79
B. Patterns of Sulfidation in the Presence of Coal Char	79
C. Effect of Char Composition on the Pattern of Sulfiation	81

	Page
D. Effect of Calcium Oxide	84
E. Summary	86
F. Recommendations for Future Work	87
Acknowledgment	88
Appendix	89
Symbols	98
References	100

CHAPTER 1: INTRODUCTION

Despite the recent temporary increases in the availability of natural gas, the United States faces a shortage of natural gas and other hydrocarbon fuels during the rest of this century. Enough proven coal reserves exist in the United States to fill the gap between the demand for and the supply of energy for hundreds of years. Unfortunately since coal is a solid, it is more difficult to handle and transport than natural gas or oil. Since coal contains inorganic compounds, it does not burn completely, but forms coal char which has a high carbon content and also contains inorganic ash and sulfur. Coal could be used in a much more efficient and environmentally acceptable manner by gasifying the coal in plants located close to coal mines to produce high-BTU pipeline quality gas--which would complement natural gas--or methanol--which can be burned directly, blended with gasoline, or upgraded to high octane gasoline. Low-BTU gas, which can be burned directly for power generation, can also be produced from coal.

Several commercially proven coal gasification processes exist. These include the Lurgi and the Koppers-Totzek processes. During the 1970's, much research has been carried out in the United States to develop better, thermodynamically more efficient gasification processes. Much of this work is now at the pilot plant stage. These new processes include the Hygas, Bi-gas, Synthane, CO_2 Acceptor and Battelle-Union Carbide (B-UC) processes. These processes are described in detail in the literature[1,2,3]. All involve the reaction of coal with water and oxygen or air to form a synthesis gas, consisting of carbon monoxide, carbon dioxide, hydrogen, water, methane, hydrogen sulfide, and tars, which is scrubbed to remove the hydrogen sulfide,

carbon dioxide, and tars, and then reacted further to increase the methane content or to form methanol.

The principal difference between these new processes and the Lurgi process is that most of the new processes operate at much higher temperatures (~1255 K) than the Lurgi process (800 K). At the higher temperature, greater thermodynamic efficiency is achieved, but the gases produced are much more corrosive. The most important disadvantage of the Lurgi process is that it is presently limited to non-caking coals. The disadvantages of the Koppers-Totzek process are that it operates at atmospheric pressure and is difficult to scale up.

Process diagrams for two of the new processes, the Synthane process and the FMC-CoEd process, are shown in Figures 1 and 2, respectively. A comprehensive summary of process diagrams for many other processes is presented in Reference 3.

Since coal contains significant amounts of sulfur, sulfidation of coal gasifier internals can be expected. Both the gas produced during gasification and the char by-product, which consists of inorganic ash and unreacted carbon, contain enough sulfur to cause severe corrosion problems and in some cases catastrophic failure of the equipment. The exact compositions of the char and the gas depend on the specific process, the operating conditions (i.e., the pressure and temperature), and the coal used. The estimated gas compositions of five processes are listed in Table I. The equilibrium oxygen and sulfur partial pressures of these gases are strongly temperature dependent (see Figures 3 and 4, respectively). The composition of the char and ash formed in the Synthane process from Illinois #6 coal, which is typical, is presented in Table II.

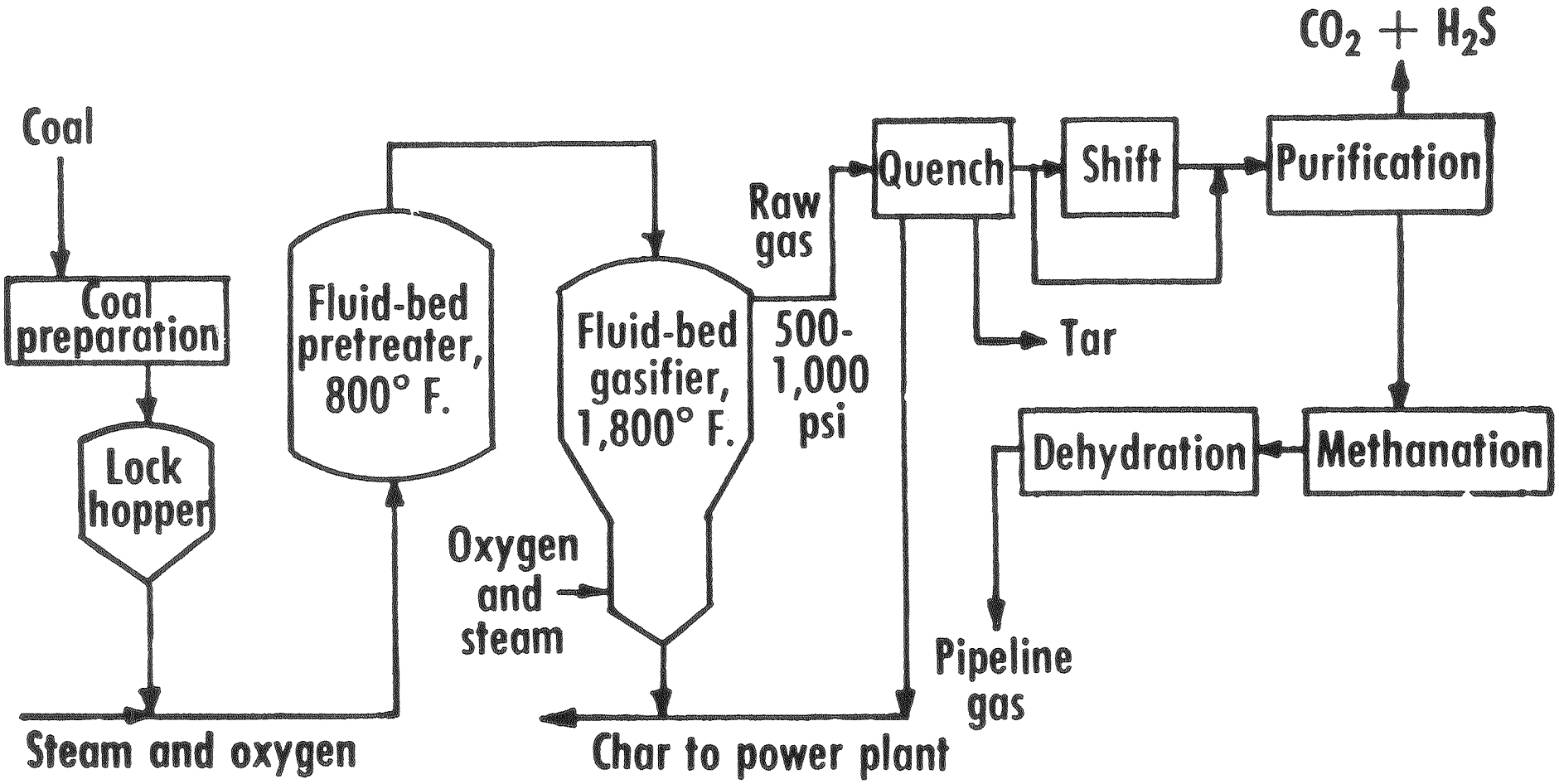

Figure 1: Process Diagram of the Synthane Coal Gasification Process (from Ref. 3)

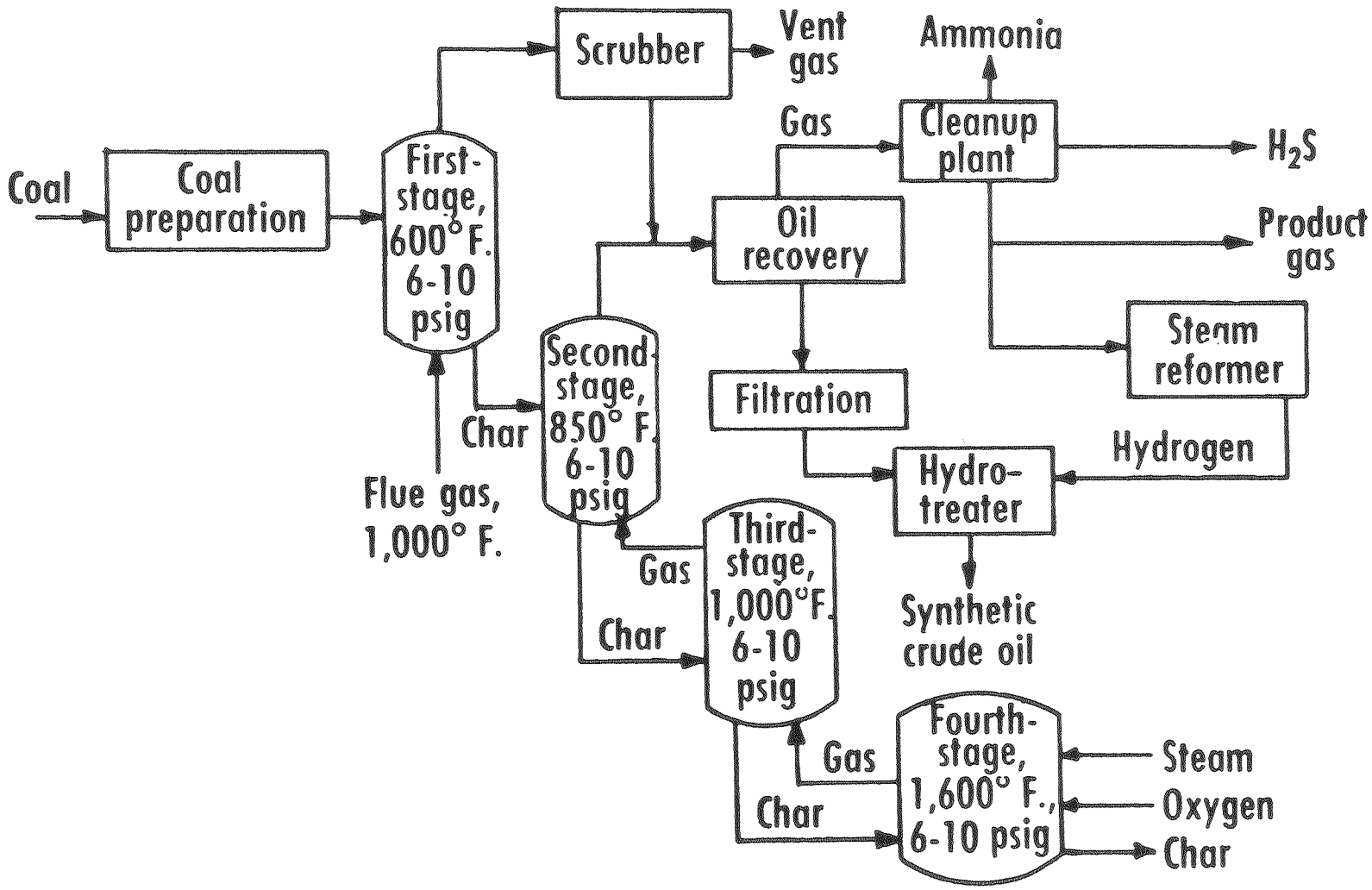

Figure 2: Process Diagram of the FMC-CoEd Coal Gasification Process (from Ref. 3)

Table I. Estimated Gas Compositions (Vol %) and Temperature and Pressure Conditions in Various Coal-gasification Processes with Low-sulfur Coal Feedstock*

Parameters	HYGAS	CO_2 Acceptor	Synthane	Battelle-Union Carbide	Bi-gas
H_2	17	52	19	49	15
CO	21	11	9	26	12
CO_2	21	6	21	5	13
CH_4	15	3	12	6	7
H_2O	25	28	36	14	52
H_2S	0.1	0.03	0.1	0.3	0.5
NH_3	1	1	1	1	1
P, psi (atm)	1200 (80)	300 (20)	1000 (70)	100 (7)	1000 (70)
T, °C (°F)	955 (1750)	870 (1600)	982 (1800)	982 (1800)	927 (1700)

*From Ref. 4; Conversion factors: 1 atm - 0.101356 MPa; T K = T°C + 273

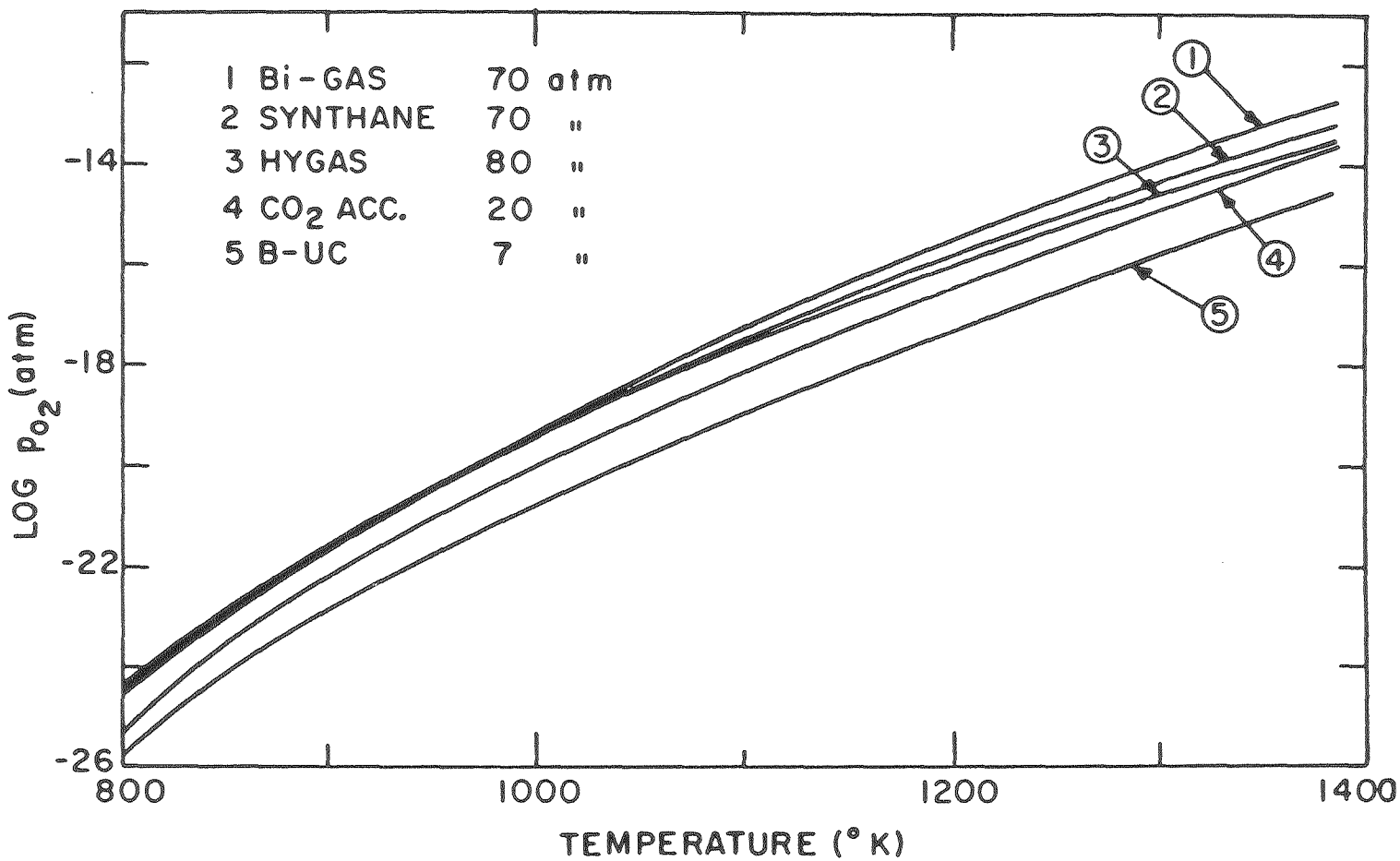

XBL 794-9394

Figure 3: Equilibrium Oxygen Partial Pressures of Five Coal Gasification Processes (from Ref. 4)

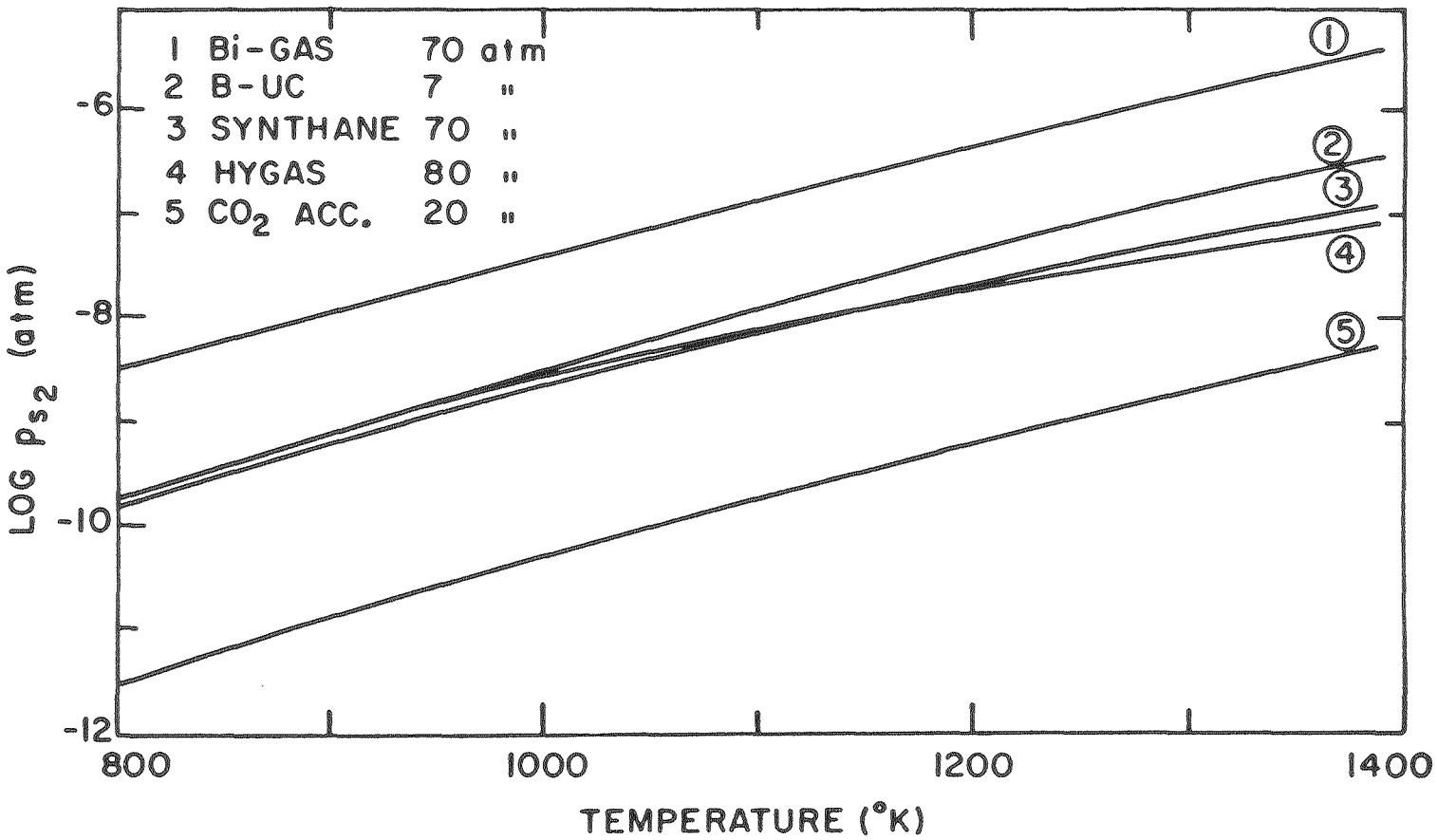

XBL 794-9395

Figure 4: Equilibrium Sulfur Partial Pressures of Five Coal Gasification Processes (from Ref. 4)

Table II: Composition of Illinois #6 Ash and Coal Char*

ASH	Percentage
SiO_2	46.3
Al_2O_3	15.2
Fe_2O_3	14.9
CaO	6.5
MgO	1.1
TiO_2	0.6
P_2O_5	0.2
Na_2O	3.0
K_2O	1.8
SO_3	5.4
	as sulfate

CHAR	Percentage
carbon	25-50%
ash	45-70%
sulfur	<1.5%
high boiling tars	<4.0%

*from Ref. 5

In this work the physical and chemical interactions between the bulk gas and coal char, and their effect on the sulfidation of metal alloys, are studied.

A. Thermodynamics of Sulfidation and Oxidation

The thermodynamics of scale formation have been studied extensively. Birks presents an excellent discussion of the thermodynamics of simultaneous oxidation and sulfidation.[6] Thermodynamic equilibrium stability diagrams which predict the stable compounds as a function of sulfur and oxygen partial pressures and temperature best summarize the thermodynamic data. The stability diagrams for 304 stainless steel, an Fe-Ni-Cr alloy, at three typical coal gasifier temperatures, are presented in Figure 5. Stability diagrams for pure iron, chromium, and nickel in oxidizing/sulfidizing environments at 1200 K are superimposed in Figure 6.

Stability diagrams for other alloys have been published[7,8]. The usefulness of these diagrams is limited, since kinetic restrictions may prevent the formation of some stable compounds. It is also important to note that these predictions are based on local conditions. The partial pressures in the scale will differ considerably from those at the scale surface or in the bulk gas. For example, the oxygen partial pressure in an oxide scale decreases from a maximum at the scale surface to a minimum at the scale-bulk metal interface. If the scale is not protective, sulfur can diffuse through the scale or along grain boundaries, and internal sulfides may become stable. A region of the alloy may be depleted of one of the elements due to outward cation diffusion through the scale, thereby changing the activities of the metals in the alloy and the scale. Therefore, since the local

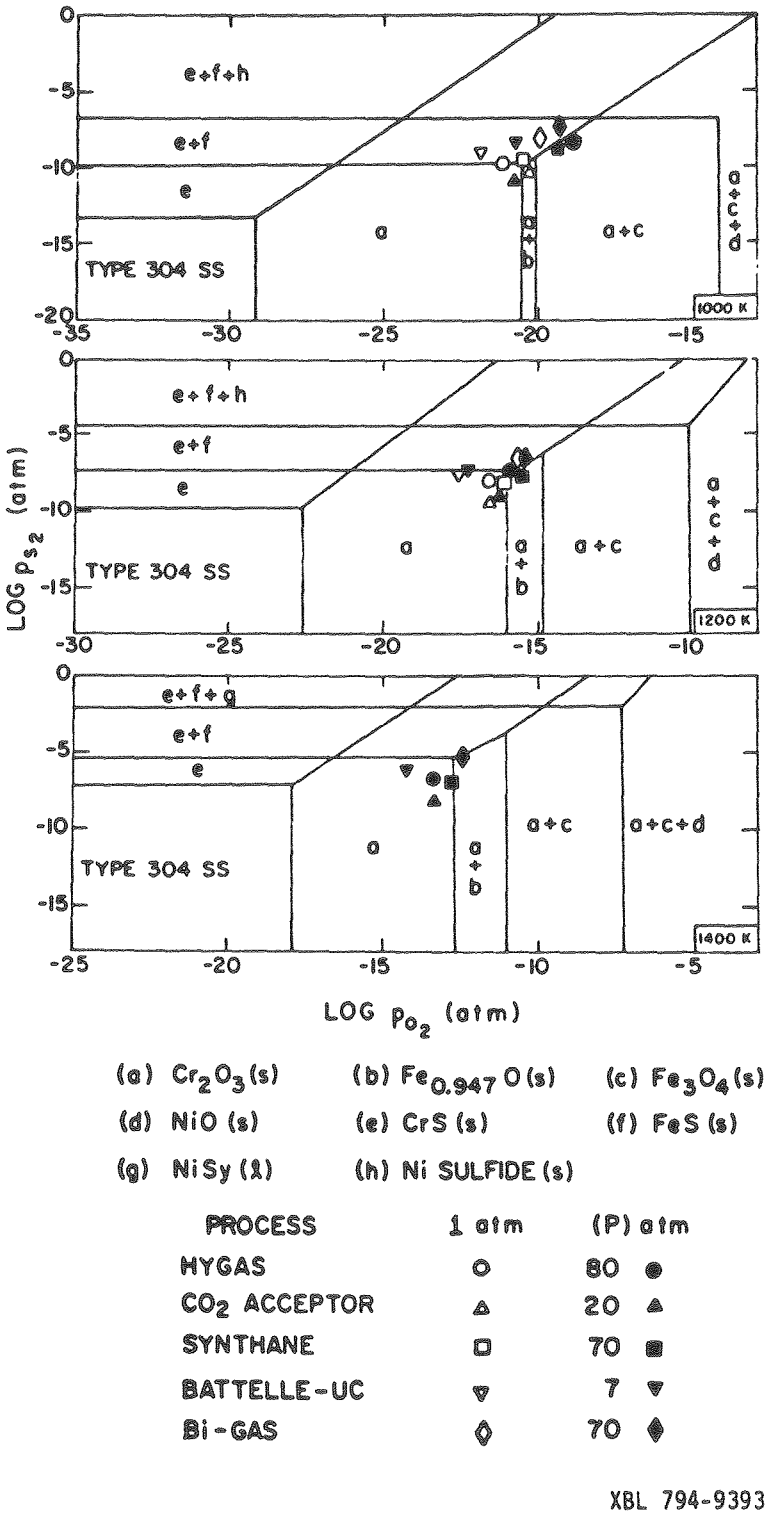

Figure 5: Thermodynamic Stability Diagrams of 304 Stainless Steel at 1000 K, 1200 K, and 1400 K (from Ref. 4)

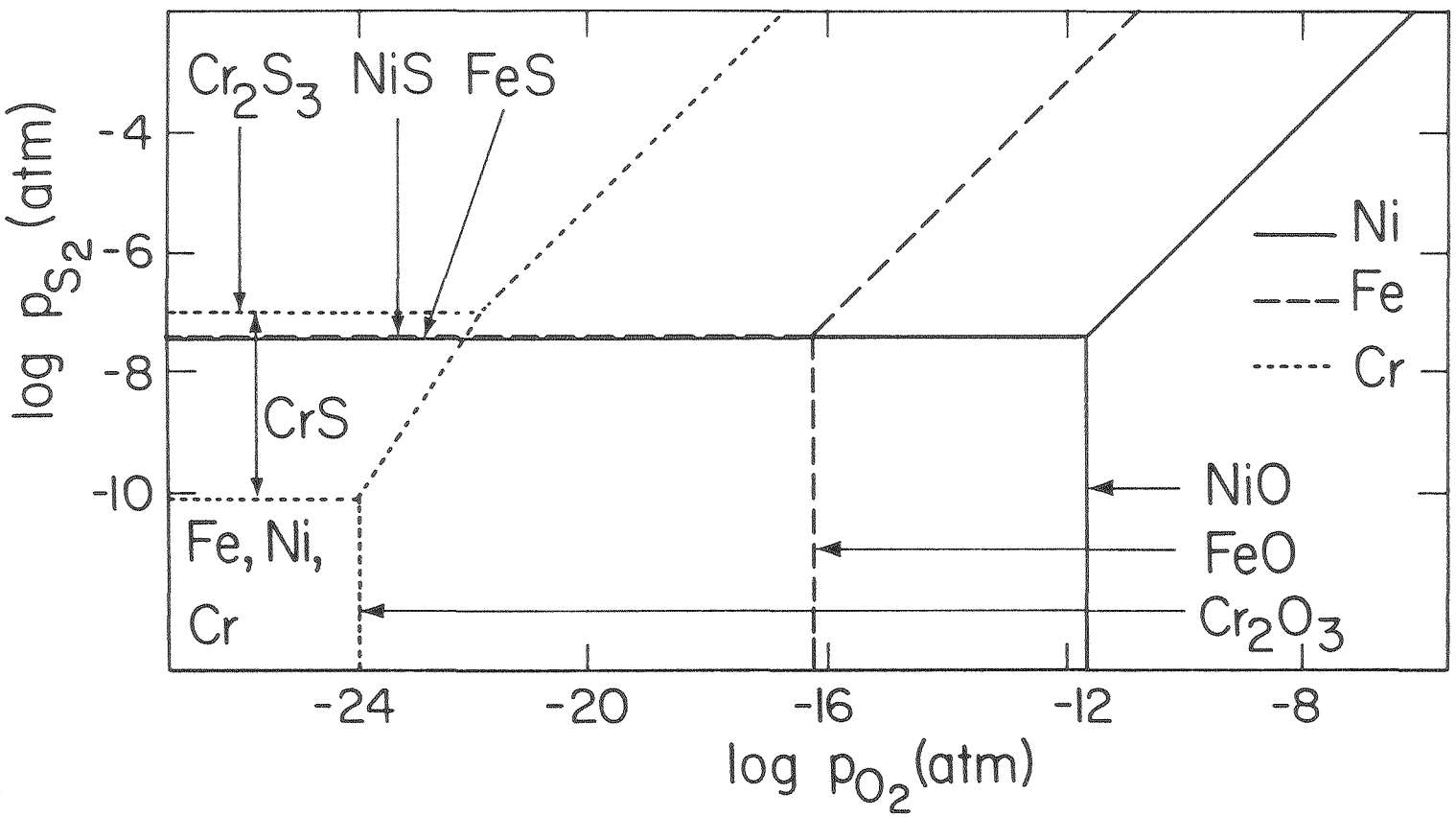

XBL 796-1691

Figure 6. Superimposed Thermodynamic Stability Diagrams of Iron, Nickel, and Chromium at 1200 K

conditions in the scale vary, simultaneous oxidation and sulfidation often occurs.

B. Mechanism and Kinetics of Oxidation/Sulfidation

Little is known about the kinetics of simultaneous oxidation and sulfidation. Most mechanistic explanations of the observed corrosion are qualitative and based on thermodynamics. The effects of a sulfide or oxide scale on the sulfur and oxygen pressures within the scale and the resulting switch from oxidation to sulfidation, or vice versa, have already been explained. It has been observed experimentally that if the oxygen partial pressure is at least 1000 times greater than the oxygen partial pressure determined by the sulfide/oxide equilibrium and the sulfur partial pressure of the gas at the metal surface, reasonable long term resistance to internal sulfidation occurs. However, even under these conditions internal sulfidation occurs after very long exposure times[4].

Most of the accurate measurements of the kinetics of scale growth have been carried out in gaseous atmospheres for pure oxidation or sulfidation. Some experiments with oxidizing/sulfidizing gases at high oxygen partial pressures have also been performed[9]. The kinetics of scale growth in oxidizing/sulfidizing gases have not been measured at the low oxygen partial pressures encountered in coal gasifiers.

If adherent scales are formed, the rate of scale growth usually follows parabolic kinetics for both sulfidation and oxidation. In other words, the square of the weight gain is proportional to the exposure time

$$(\Delta W)^2 = k_p t$$

Parabolic kinetics imply that the rate of scale formation is controlled by the outward diffusion of cations through the scale, or by the inward diffusion of oxygen or sulfur through the scale. If the scales are protective, the inward diffusion of sulfur or oxygen is much smaller than the outward diffusion of metal cations. At 1200 K a typical value of k_p for chromium sulfide scales is 10^{-6} g^2 cm^{-4} s^{-1}. The k_p for chromium oxide scales at 1200 K is about 10^{-10} g^2 cm^{-4} s^{-1}. The parabolic rate constants for iron oxide and sulfide scales are approximately 1000 times larger than the respective parabolic rate constants for chromium scales[10].

C. Previous Work on the Effect of Char on Corrosion

Most of the published research on sulfidation and oxidation of metals has been concerned with corrosion by gases. Recently Gordon[5,11] and Douglass and Bhide[12,13] have demonstrated that char can also cause sulfidation of metals. Gordon demonstrated that internal sulfides form in samples consisting of an experimental Fe-10Al alloy exposed to Synthane char. No sulfidation was observed in experimental Fe-10Al-Cr alloys and commercial 310 SS exposed to Synthane char. Gordon also exposed these metals to synthetic chars consisting of alumina and iron sulfide or calcium sulfate. He then exposed the metals to these "chars" in sulfur free gases. The oxygen partial pressures of these gases were 10^{-15} atm and 10^{-19} atm. For the experiments at the lower oxygen partial pressure, graphite was added to the synthetic chars. He observed that the iron sulfide char is more sulfidizing at the high oxygen partial pressure than at the lower one. With calcium sulfate char the opposite trend is observed. More sulfidation occurs at the lower oxygen partial pressure than at the higher one. Based on the

morphology of the corrosion products formed, Gordon concluded that iron sulfide is the primary sulfur containing species in char.

Bhide and Douglass demonstrated that the corrosion of alloys by coal char depends strongly on the experimental conditions. They exposed samples to a finite amount of FMC char in a closed system. In such a system the sulfur in the char will equilibrate with the atmosphere, and subsequently the sulfur partial pressure will drop as the sulfur reacts with the metal. If the sulfur partial pressure drops enough, oxides become stable. This was observed experimentally. Both sulfides and oxides were formed when samples were exposed for 96 hours to FMC char which was not replenished. On the other hand, only sulfides formed on samples exposed for 96 hours if the char was replaced with fresh char every 12 hours.

Bhide and Douglass also demonstrated that the extent and rate of corrosion increase as the quantity of FMC char to which a sample is exposed in a closed environment increases. Results for Inconel 671 exposed to FMC char at 1255 K (1800 °F) are presented in Figure 7.

Neither Gordon nor Bhide observed any carburization of the samples. Both observed that char particles were imbedded in the scale as it grew outward, making it less coherent.

D. Objectives

The discussion of the thermodynamics and mechanisms of corrosion demonstrated that the corrosion of metals depends on the local conditions at the metal surface, the alloy composition, and the composition and morphology of the sulfides and oxides formed. The local conditions at the alloy surface depend on the bulk gas composition and the composition and physical properties of the char. The purpose of this

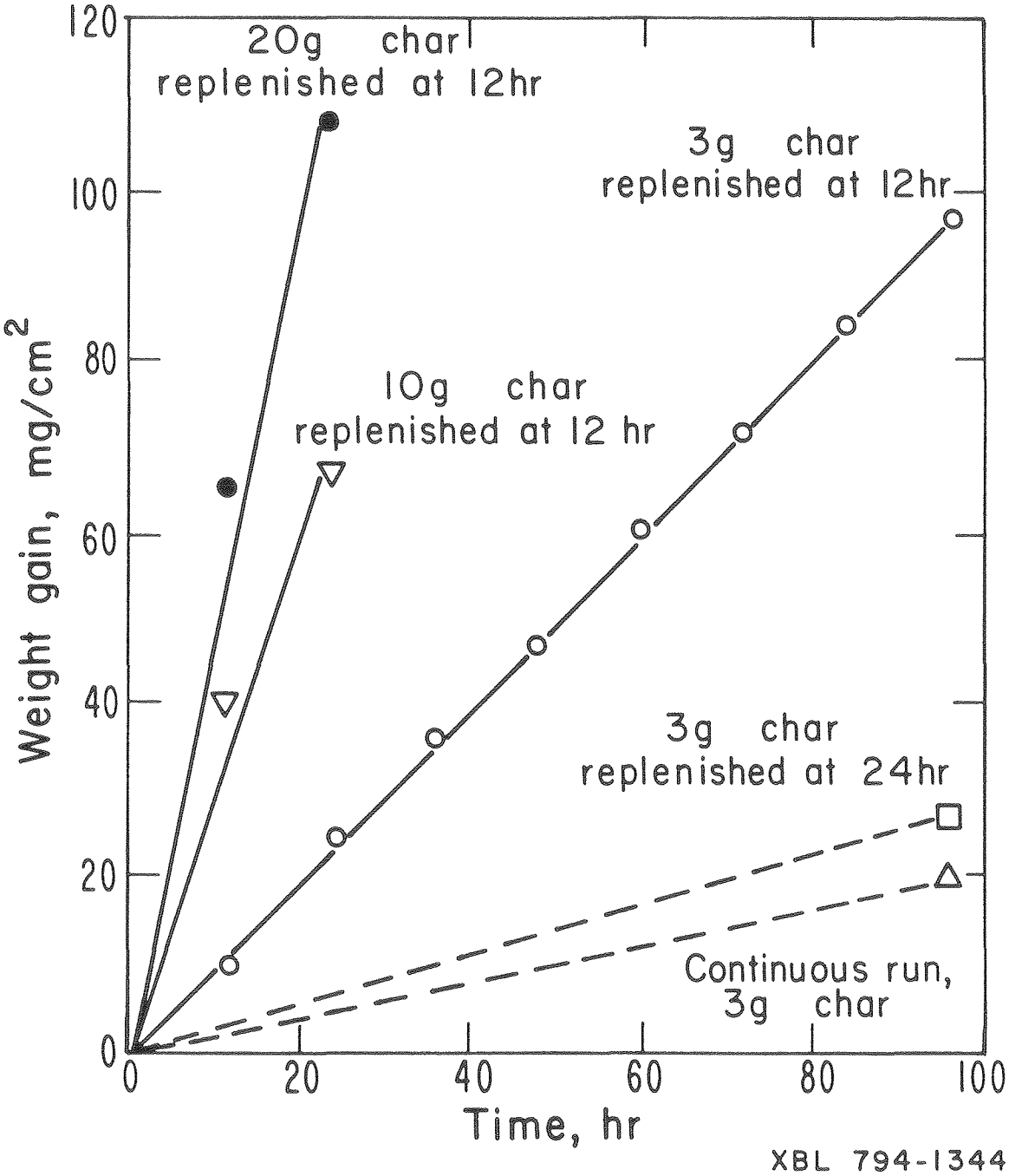

Figure 7: Weight Gains of Inconel 671 Exposed to FMC Char at 1255 K (from Ref. 13)

project is to show how the gas composition at the metal surface differs from the bulk gas composition because of a layer of coal char covering the metal surface.

The sources of the sulfur which diffuses to the metal surface are the bulk gas and/or the char. The char can increase the rate of corrosion by serving as a source of sulfur, or it can reduce the amount of corrosion by reducing the sulfur partial pressure at the metal surface because of the concentration gradient through the char or by reacting with the sulfur in the gas phase to reduce the sulfur content of the gas phase at the metal surface. Char also reduces the oxygen partial pressure at the char-metal interface and thus the formation of protective oxide scales. Char properties which affect the sulfidation/oxidation of metals include the composition, depth, porosity, and reactivity of the char.

Other factors which influence the rate of corrosion are the composition and flow rate of the bulk gas over the char surface. If the bulk gas contains little or no sulfur and is flowing over the char at a rapid rate, some of the sulfur formed in the char will diffuse out to the bulk gas, rather than to the metal. On the other hand, if the gas above the char does not move, as in Douglass and Bhide's apparatus, the only source of sulfur is the char, and since none of the sulfur is removed by convection of the bulk gas, most of it will react with the metal.

In this project the effects of char composition and depth and bulk gas composition and flow rate on the corrosion of 304 stainless steel are investigated. A model which predicts the concentration profiles and fluxes of the gaseous species in the char is developed. These

variables are also studied experimentally by exposing metal coupons to the corrosive char-gas environment and examining the corrosion products formed.

CHAPTER 2: MODEL OF MASS TRANSFER THROUGH COAL CHAR

As discussed previously, the presence of coal char can significantly affect the corrosion of metals in a corrosive atmosphere. In this chapter a simple model predicting the composition profile of the gas in the char is developed. It is solved to predict the effect of such variables as char composition, char depth, and bulk gas composition on the rate of sulfidation.

A. Assumptions

The system modeled is presented in Figure 8. This figure also explains the coordinate system and the relevant variables. Convection of the bulk gas maintains a constant composition at the char-gas interface (z=L). Some of the bulk gas diffuses through the char to the metal surface (z=0) where it reacts. The composition of the gas in the char varies because of diffusion gradients and homogeneous gas phase reactions and heterogeneous reactions between the char and the gas phase. Radial effects are neglected to make the governing differential equations one-dimensional. A constant temperature and ideal-gas behavior are assumed for the gas phase. The quantity of char which reacts with the gas is small enough that the porosity of the char is constant.

B. Governing Equations

Table III lists the governing equations which describe the diffusion of a multicomponent gas mixture through a packed bed. The relevant variables are defined there also. The Stefan-Maxwell equations (1) relate the fluxes of the gaseous species to their mole fraction gradients. Equation 2 is the overall hydrogen balance which defines the fluxes. The $\nu_{i,H}$ are the stoichiometric coefficients of

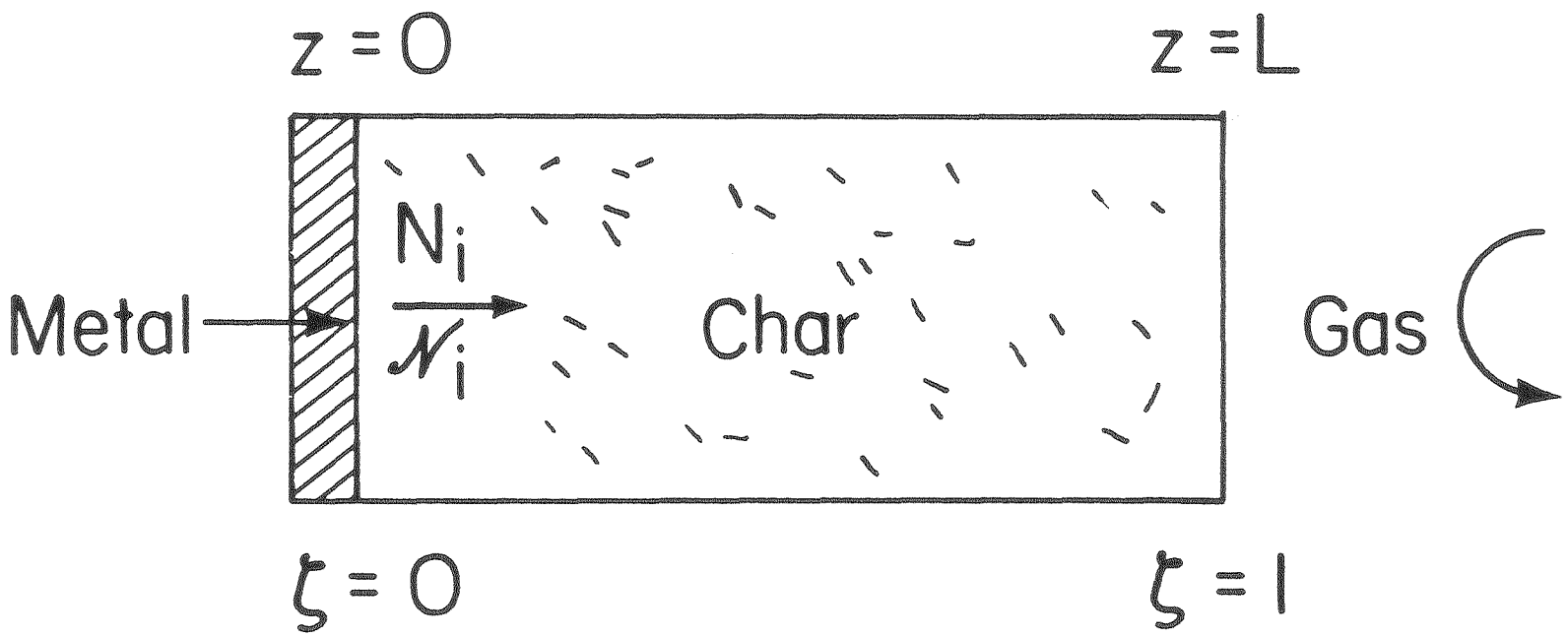

XBL 795-1675

Figure 8. The System Modelled in Chapter 2.

Table III: Governing Equations for Multicomponent Diffusion Through Coal Char

Equation		Number of Equations
$\nabla x_i = \sum_{j \neq i} \frac{1}{cD_{ij}} (x_i N_j - x_j N_i)$	(1)	(n-1)
$\sum_i \nu_{i,H} N_i = 0$	(2)	1
$\nabla \cdot N_i = R_i$	(3)	(n-1)
$\sum_i x_i = 1$	(4)	1
	Total	2n

$\nabla = \frac{\partial}{\partial \zeta}$ = dimensionless differential operator

R_i = rate of formation of species i (mol cm^{-3} s^{-1})

$\mathcal{R}_i = L^2 R_i$ (mol cm^{-1} s^{-1})

hydrogen in species i. Since hydrogen does not leave the gas phase, and there is no accumulation at steady state, the total hydrogen flux must be zero throughout the char. The mole balances (3) relate the fluxes to the rates of the reactions which depend on the composition of the gas phase.

These equations are solved using an approach developed by Newman[14]. The Stefan-Maxwell equations are rewritten as

$$-N_i \sum_{j \neq i} \frac{x_j}{cD_{ij}} + \sum_{j \neq i} N_j \frac{x_i}{cD_{ij}} = \nabla x_i \tag{5}$$

The matrix of coefficients defined by Equation 5 and Equation 2 can be inverted to express the fluxes in terms of the gradients of the mole fractions.

$$N_i = \sum_{k=2}^{n} b_{ik} \nabla x_k \tag{6}$$

If the exact mole fractions are not known, Equation 5 must be linearized before it is inverted. Equation 6 is then replaced by

$$N_i = \sum_{k=2}^{n} b_{ik} [\nabla x_k - \Delta x_k \sum_{j \neq k} \frac{N_j^o}{cD_{kj}} + N_k^o \sum_{j \neq k} \frac{\Delta x_j}{cD_{kj}}] \tag{7}$$

where $\Delta x_k = x_k - x_k^o$, and the N_k^o are the fluxes based on the best available estimates of the mole fractions, x_k^o. The b_{ik} in Equation 7, which are also based on the best estimates of the mole fractions, are the same as those in Equation 6.

Differentiation of the Stefan-Maxwell equations and substitution of Equations 3 and 7 yields

$$\nabla^2 x_i = \sum_{j\neq i} \frac{x_i R_j - x_j R_i}{cD_{ij}}$$

$$+ \sum_{j\neq i} \nabla \frac{x_i}{cD_{ij}} \cdot \sum_{k=2}^{n} b_{jk} \left[\nabla x_k - \Delta x_k \sum_{l\neq k} \frac{N_l^o}{cD_{kl}} + N_k^o \sum_{l\neq k} \frac{\Delta x_l}{cD_{kl}}\right]$$

$$- \sum_{j\neq i} \nabla \frac{x_j}{cD_{ij}} \cdot \sum_{k=2}^{n} b_{ik} \left[\nabla x_k - \Delta x_k \sum_{l\neq k} \frac{N_l^o}{cD_{kl}} + N_k^o \sum_{l\neq k} \frac{\Delta x_l}{cD_{kl}}\right] \tag{8}$$

The linearized form of these equations is

$$\nabla^2 x_i - \sum_{j\neq i} \frac{x_i R_j - x_j R_i}{cD_{ij}} - N_i^o \, S1 =$$

$$- \sum_{k=2}^{n} \nabla x_k \left[b_{ik} S1_i - S3_{k,i}\right]$$

$$+ \sum_{k=2}^{n} \Delta x_k \, S2_k (S1_i b_{ik} - S3_{k,i})$$

$$+ \sum_k \Delta x_k \sum_{l\neq k} \frac{N_l^o}{cD_{kl}} (S3_{l,i} - b_{il} S1_i)$$

$$+ \Delta\sum_{l\neq i} \nabla\left(\frac{x_i}{cD_{il}}\right) \cdot N_l^o - \sum_{k\neq i} \nabla \frac{x_k}{cD_{ik}} N_i^o \tag{9}$$

$$S1_i = \sum_{l\neq i} \nabla \frac{x_l^o}{cD_{il}} \tag{10}$$

$$S2_i = \sum_{l\neq i} \frac{N_l^o}{cD_{il}} \tag{11}$$

$$S3_{1,k} = \sum_{i \neq k} b_{i1} \nabla \frac{x_k^o}{cD_{ki}} \tag{12}$$

These equations and Equation 4 are then solved iteratively until the mole fractions are converged.

C. Physical Properties

In order to solve Equations 4, 9, 10, 11, and 12, the diffusion coefficients in a porous medium, D_{ij}, and the rate expressions, R_i, must be known.

The diffusion coefficients can be expressed as a function of the ordinary binary diffusion coefficients, $\mathcal{D}_{ij}$, and the void fraction, ε, of the char. If N_i (or $\mathcal{N}_i$) is the flux per unit area, averaged over the entire cross section, then D_{ij} can be written as[15]

$$D_{ij} = \varepsilon^{n+1} \mathcal{D}_{ij}$$

Values of 0.4 and 0.5 will be assumed for ε and n, respectively. Therefore

$$D_{ij} = 0.253\, \mathcal{D}_{ij}$$

The ordinary binary diffusion coefficients are correlated in terms of their Lenard-Jones parameters[16]

$$c\mathcal{D}_{AB} = 2.2646 \times 10^{-5} \frac{\sqrt{T(1/M_A + 1/M_B)}}{\sigma_{AB}^2\, \Omega_{\mathcal{D}_{AB}}}$$

The collision integral, $\Omega_{\mathcal{D}_{AB}}$, is a function of the dimensionless temperature, kT/ε_{AB}. The Lenard-Jones parameters of the pair A-B, σ_{AB} and ε_{AB}, can be approximated by the following empirical mixing rules

from the Lenard-Jones parameters of pure A and B.

$$\sigma_{AB} = \frac{1}{2}(\sigma_A + \sigma_B) \qquad \varepsilon_{AB} = \sqrt{\varepsilon_A \varepsilon_B}$$

The Lenard-Jones parameters of many species have been measured and are listed in many textbooks[15,16]. For species whose Lenard-Jones parameters have not been measured, values can be estimated from the normal boiling point (K) and the molar volume (cm^3/mol), at the normal boiling point[17]

$$\sigma = 1.18\ V_b^{1/3} \qquad \frac{\varepsilon}{k} = 1.15\ T_b$$

Since little kinetic data for char-gas reactions and gas-phase reactions in the presence of char are known, it is assumed that the rates of the reactions are large enough that local equilibrium will exist in the char. Any mass-transfer limitations due to mass transfer of the gaseous species to and from the surface of the char particles will be neglected. These assumptions are reasonable because of the high temperatures in coal gasifiers. If the kinetic data become available, they can of course be included.

For simple reversible reactions, the net rate of the reaction can be expressed as

$$R_j = r_{jf} - r_{jb} = k_{jf} \prod_{react} x_i^{\nu_i} - k_{jb} \prod_{prod} x_i^{-\nu_i}$$

Since at equilibrium the forward and backward rates of reaction must be equal, only one of the rate constants is independent. Thus

$$R_j = k_{jb}(K_j \prod_{react} x_i^{\nu_i} - \prod_{prod} x_i^{\nu_i})$$

For large k_{ib} the reaction will be forced to equilibrium. The gas phase and char-gas reactions will be discussed in more detail below.

The equilibrium constants are calculated from the Gibbs energies for the reactions. These data have been tabulated as a function of temperature in the JANAF Tables[18] and other sources[19] for many compounds. They are calculated from standard Gibbs energy, enthalpy of formation, and heat capacity data.

$$\frac{d}{dT}\left(\frac{\Delta G^o}{RT}\right) = -\frac{\Delta H^o}{RT^2} \qquad \Delta H^o = \Delta H_o + \int_{T_o}^{T} \Delta C_p^o \, dT$$

The binary diffusion coefficients and equilibrium constants at 1200 K of the species considered in this work are listed in Tables IV and V, respectively.

D. Boundary Conditions

For a system of n gaseous species, 2n boundary conditions must be specified to define a unique solution, since the differential equations are second order. At the char-gas interface (z=L), the composition of the gas phase is specified. In order to eliminate kinetic effects, equilibrium concentrations are chosen. At the char-metal interface (z=0), the fluxes are specified. The dependence of the reactions between the alloy and the gas phase on the gas composition at the metal surface is not well known. Therefore the flux of hydrogen sulfide at the char-metal interface, which depends on the kinetics of the metal-gas reactions, will be treated as a parameter.

E. Solution of Governing Equations

The linearized equations are solved by approximating the differential operators with finite difference operators accurate to order h^2,

Table IV: Ordinary Binary Diffusion Coefficients of Selected Pairs at 1200 K*

	CO	CO_2	CH_4	H_2O	H_2S	O_2	S_2
CO_2	1.71×10^{-5}						
CH_4	2.40×10^{05}	1.93×10^{-5}					
H_2O	2.75×10^{05}	2.10×10^{-5}	2.86×10^{-5}				
H_2S	1.89×10^{-5}	1.47×10^{-5}	2.10×10^{-5}	2.31×10^{-5}			
O_2	2.20×10^{05}	1.70×10^{-5}	2.45×10^{-5}	2.82×10^{-5}	1.92×10^{-5}		
S_2	1.09×10^{-5}	$.808 \times 10^{-5}$	1.26×10^{-5}	1.20×10^{-5}	$.816 \times 10^{-5}$	1.09×10^{-5}	
H_2	7.97×10^{-5}	6.78×10^{-5}	7.66×10^{-5}	9.47×10^{-5}	7.32×10^{-5}	8.38×10^{-5}	4.55×10^{-5}

*tabulated here is $c\mathcal{D}_{ij}$ (mol $cm^{-1}s^{-1}$)

Table V: Equilibrium Constants for Formation from the Elements of Selected Compounds at 1200 K

Compound	Log K_P
CO	9.47
CO_2	17.20
H_2O	7.90
H_2S	1.36
CH_4	-1.80
CaS	18.07
CaO	22.12
$CaSO_4$	41.62
FeS	3.83
FeO	8.46
$FeSO_4$	21.29

and solving the resulting set of linear algebraic equations iteratively. The difference operators are listed in Table VI.

Finite difference approximations of Equations 4,9,10,11, and 12 are programmed at all mesh points between j=2 and j=NJ-1, inclusively. At j=1, the char-metal interface, the specified fluxes are substituted into the Stefan-Maxwell equations, and the resulting equations are programmed directly. At j=NJ, the char-gas interface, the concentrations of the gas phase are fixed.

The finite difference equations are set up using a slightly modified version of COMPOS, a subroutine written by Newman. The matrix of the coefficients of the finite difference equations is a tridiagonal matrix whose elements along the main diagonals are n x n matrices. These equations can be solved efficiently by using BAND, another subroutine written by Newman. Printouts of these programs are presented in the appendix.

F. Thermodynamics of Char-Gas Reactions

Several reactions are possible between char and the gas phase. If the char is not completely devolitalized, the volatiles will be driven off because of the high temperature. If these volatiles contain sulfur they can significantly increase the sulfur pressure in the char.

Carbon in the char is oxidized to CO and CO_2. At 1200 K the equilibrium constants for these reactions are

$$K_{CO} = 2.95 \times 10^{9} = \frac{p_{CO}}{p_{O_2}^{1/2}}$$

$$K_{CO_2} = 1.58 \times 10^{17} = \frac{p_{CO_2}}{p_{O_2}}$$

Table VI: Finite Difference Operators

$$\nabla c = \frac{c(j+1) - c(j-1)}{2h} + O(h^2)$$

$$\nabla^2 c = \frac{c(j+1) - 2c(j) + c(j-1)}{h^2} + O(h^2)$$

At boundaries

$$\nabla c = \frac{-3c(1) + 4c(2) - c(3)}{2h} + O(h^2)$$

Therefore, since char contains significant amounts of carbon, the equilibrium oxygen partial pressure is less than 10^{-18} atm. At these low oxygen partial pressures, sulfur dioxide and sulfur trioxide are unstable, therefore hydrogen sulfide is the only significant gaseous sulfur containing species.

Char also contains ash which consists of inorganic oxides, sulfides, and sulfates. Both iron sulfide (FeS) and calcium sulfate ($CaSO_4$) have been postulated as the primary sulfur containing species in char[11]. Simplified stability diagrams of the calcium-sulfur-oxygen and iron-sulfur-oxygen systems at 1200 K are presented in Figures 9 and 10, respectively. At 1200 K, $CaSO_4$ is unstable at the low oxygen partial pressures ($p_{O_2} < 10^{-18}$ atm) in coal char. The sulfur partial pressure determines whether $CaSO_4$ decomposes to calcium oxide (CaO) or calcium sulfide (CaS). For example, if the oxygen partial pressure is 10^{-19} atm, and the sulfur partial pressure is 10^{-8} atm, $CaSO_4$ will decompose to form CaS, and thus not affect the sulfur pressure. At the same oxygen partial pressure and a sulfur partial pressure of 10^{-12} atm, $CaSO_4$ will decompose to form CaO until the sulfur pressure has risen to the pressure corresponding to the CaO/CaS equilibrium ($p_{S_2} = 10^{-11}$ atm) or all of the sulfate has reacted. Typical gasifier gas compositions are in the range where CaS is stable. Therefore any CaO in the char will react to form CaS, reducing the sulfur partial pressure.

At the low oxygen partial pressures in coal char, iron oxide is unstable, and if no other oxides are present, the sulfur partial pressure at 1200 K is fixed by the Fe/FeS equilibrium at 2×10^{-8} atm.

Thus, the effect of the ash in coal char on the sulfur pressure of the gas and the rate of sulfidation depends strongly on its composition. It can raise or lower the sulfur partial pressure of the gas in

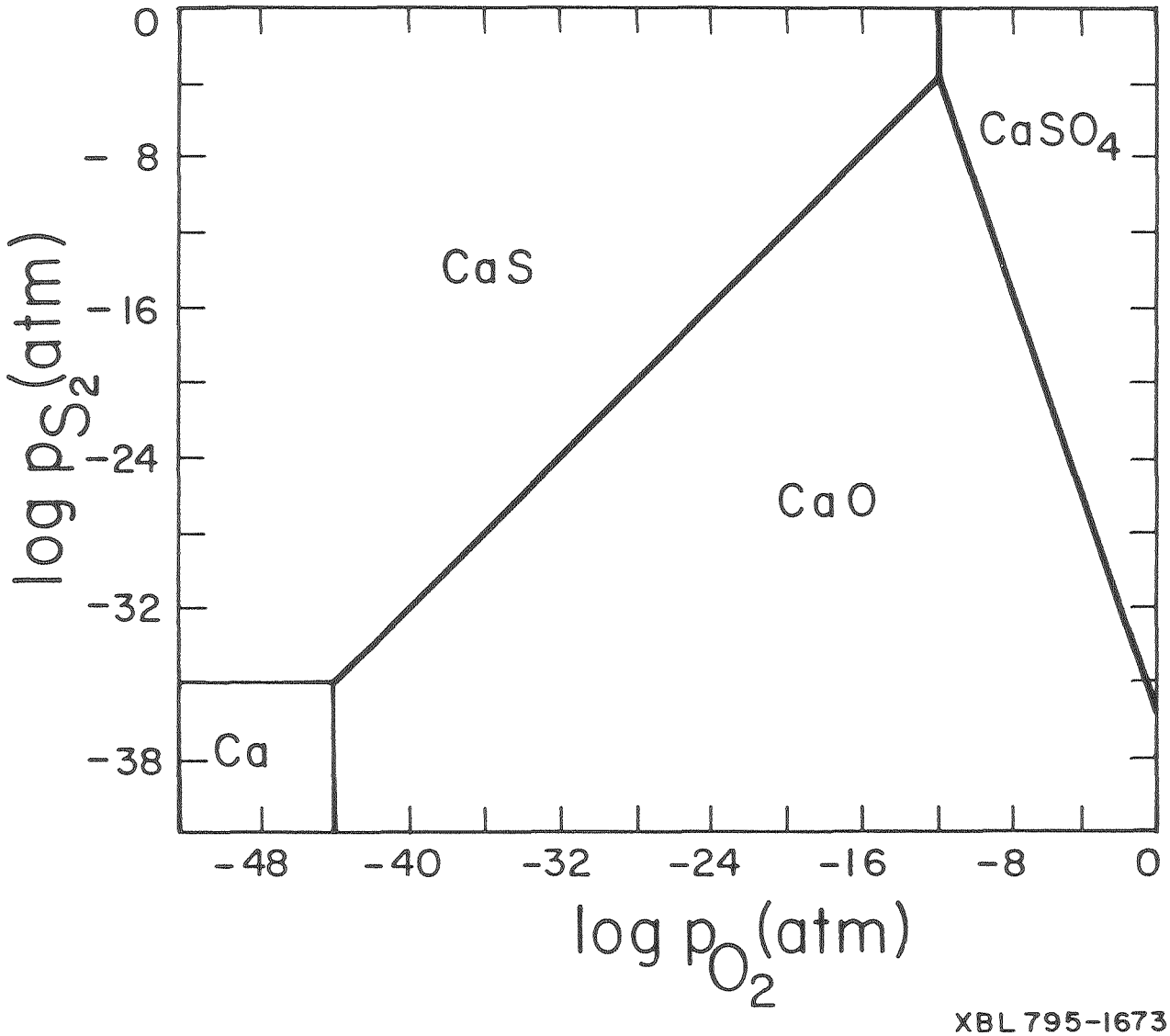

Figure 9. Simplified Stability Diagram for the Calcium-Sulfur-Oxygen System at 1200 K

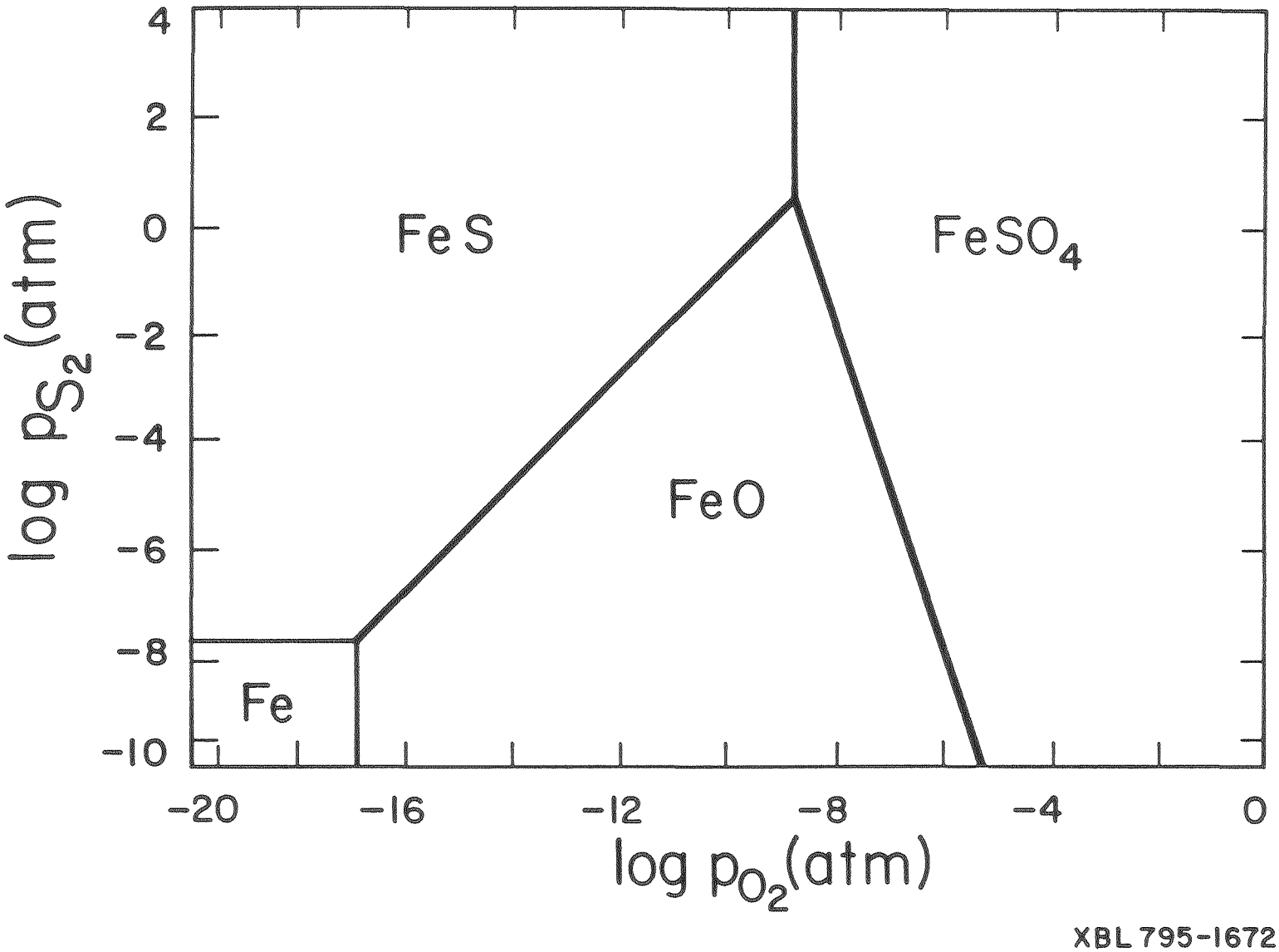

Figure 10. Simplified Stability Diagram for the Iron-Sulfur-Oxygen System at 1200 K

contact with the char, and thereby the sulfidation of metals in the char-gas environment.

G. Results for Steady State

The equations are solved by assuming that the gas phase consists of carbon monoxide (CO), carbon dioxide (CO_2), methane (CH_4), water (H_2O), hydrogen sulfide (H_2S), and hydrogen (H_2). The only reactive species in the char is carbon. Therefore, all of the sulfur in the gas phase is from the bulk gas. The following reversible char-gas reactions are assumed

$$2CO = CO_2 + C$$

$$CO + H_2 = C + H_2O$$

$$C + 2H_2 = CH_4$$

The carbon activity in the char is assumed to be one. The reaction at the char-metal interface is

$$M + H_2S \rightarrow MS + H_2.$$

This reaction is assumed to be irreversible. Because of the reaction at the metal surface, there is a flux of hydrogen sulfide to the surface and a flux of hydrogen away from it. The flux at the metal surface of all the other species is zero.

Concentration profiles. The concentrations of the species which do not react with the metal are fairly uniform throughout the char. Some of the hydrogen formed by the reaction of hydrogen sulfide and the metal reacts further to form water. Therefore, there is usually a small flux of water out of the char.

The hydrogen sulfide and hydrogen concentrations vary linearly through the char. The hydrogen sulfide concentration is a maximum at the char-gas interface, and the hydrogen concentration is greatest at char-metal interface (Figure 11). This implies that the composition variation between the char-gas interface and the char-metal interface does not significantly affect the effective diffusion coefficients of hydrogen and hydrogen sulfide in the gas mixture.

Thus, the hydrogen and hydrogen sulfide concentration profiles are determined primarily by the diffusion of hydrogen sulfide to and hydrogen away from the metal surface. The concentrations of the other species are determined by the various equilibria and the assumption that the total flux of oxygen ($= \sum_i \nu_{i,O} N_i$) is zero, since it is assumed that oxygen does not react with the metal.

Since the hydrogen to hydrogen sulfide ratio is larger at the char-metal interface than at the char-gas interface, the sulfur partial pressure ($p_{S_2} = [K_{H_2S} \frac{p_{H_2S}}{p_{H_2}}]^2$) at the char metal interface is lower than the sulfur partial pressure at the char-gas interface. This effect is discussed in more detail below.

Mass-Transfer Limits. The model can be used to calculate the maximum flux of hydrogen sulfide through the char to the metal surface. This maximum flux will be referred to as the mass-transfer limit. It usually occurs when the hydrogen sulfide concentration at the char-metal interface drops to zero. In some cases the mass-transfer limit is determined by the flux of hydrogen away from the metal surface. If the mass-transfer limit is determined by the flux of hydrogen sulfide into the char, the mass-transfer limit will be approximately linearly proportional to the hydrogen sulfide concentration at the char-gas

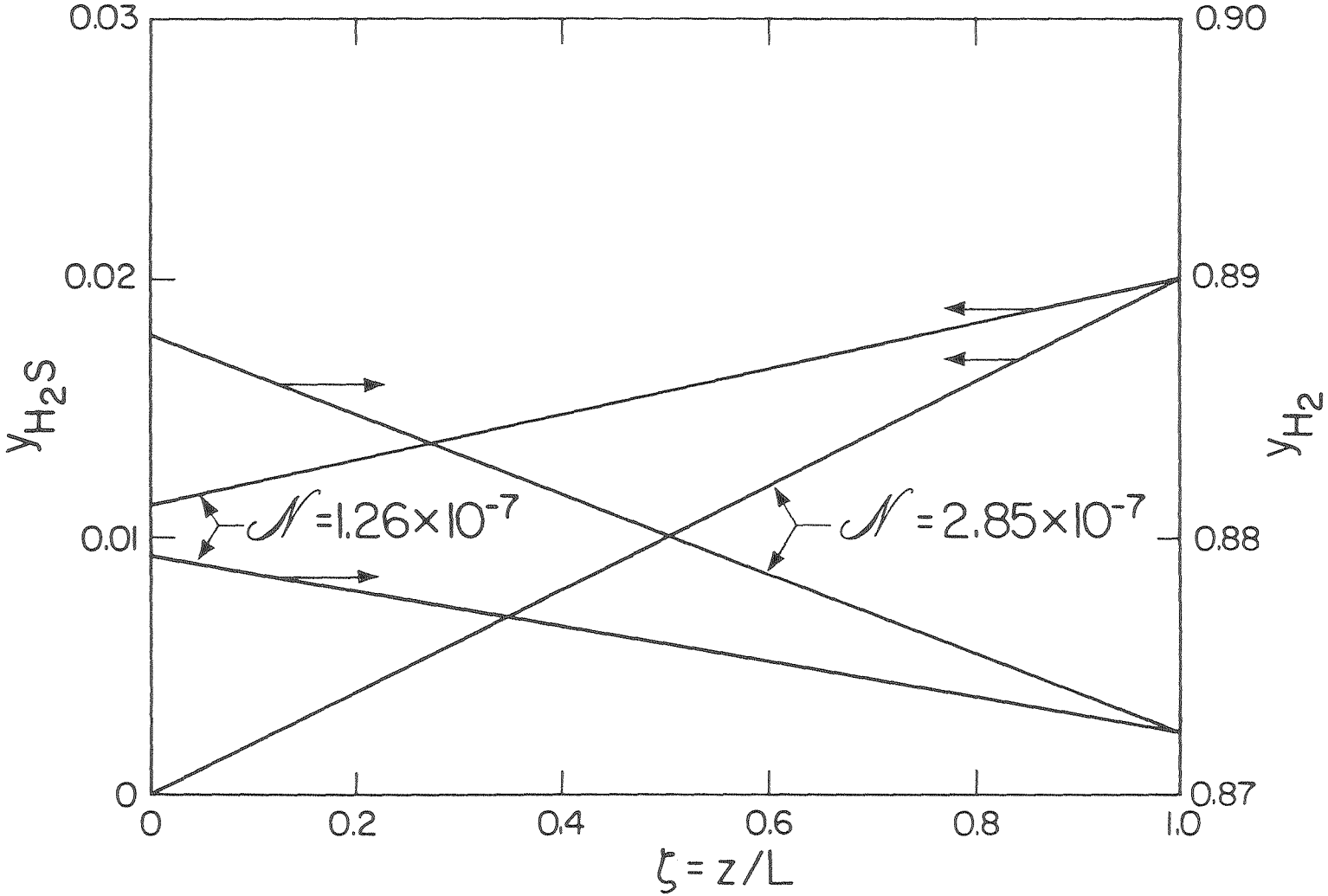

Figure 11. Concentration Profile in Ash-Free Char

XBL 795-1671

interface. It is also inversely proportional to the thickness of the char layer. In Figure 12 the mass-transfer limits are plotted as a function of the hydrogen sulfide concentration at the char-gas interface. In addition to the linear dependence of the flux on the hydrogen sulfide concentration, a slight dependence on the oxygen pressure at the char-gas interface is also observed. This probably is due to changes in the average diffusion coefficients which depend on the gas composition. At low oxygen partial pressures the bulk gas contains a lot of hydrogen, which increases the average diffusion coefficients of the species in the mixture, and thus the fluxes.

A comparison of the mass-transfer limit with the rate of sulfidation predicted by parabolic kinetics determines whether the rate of sulfidation is controlled by the diffusion of hydrogen sulfide in the char layer or controlled by the diffusion of metal cations through the scale. For a wide range of bulk gas compositions the mass-transfer limit is less than fluxes corresponding to parabolic kinetics. If the scale on the metal is thin, parabolic kinetics predict rates of scale growth much higher than the mass-transfer limit. For example, consider a metal with a $k_p = 10^{-6}\ g^2\ cm^{-4}\ s^{-1}$ at 1200 K for sulfidation. Parabolic kinetics imply that the flux of metal cations through the scale will drop to 10^{-8} mol $cm^{-2}\ s^{-1}$ only after 113 days. A comparison with Figure 12 shows that in many cases the high fluxes predicted by parabolic kinetics when the scales are thin are not possible because of the mass-transfer limit. Only after the scales are thick enough will parabolic kinetics be observed.

As discussed previously, the sulfur partial pressure at the char-metal interface decreases with increasing hydrogen sulfide fluxes.

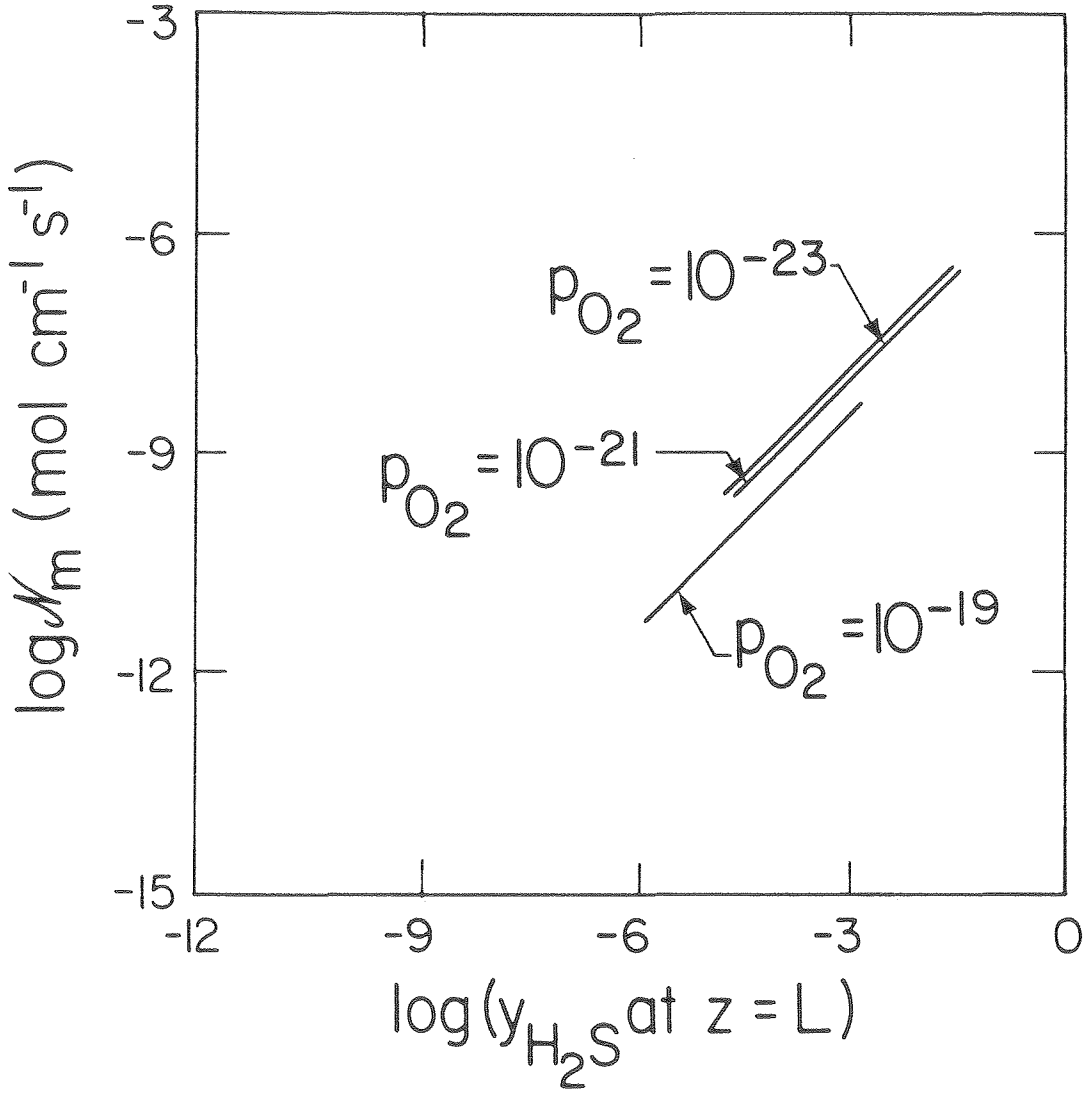

XBL 795-1669

Figure 12. Mass-Transfer Limit vs. Hydrogen Sulfide Concentration at the Char-Gas Interface

The decrease in the sulfur concentration is less than a factor of 10 for fluxes smaller than 80% of the mass-transfer limit. For larger fluxes, the sulfur pressure rapidly drops to zero (Figure 13). In real systems the decrease of the sulfur pressure at the metal surface will decrease the rate of diffusion of cations through the scale until the diffusion of hydrogen sulfide through the char equals the diffusion of metal cations through the scale. This quasi steady-state flux is greater than 80% of the mass-transfer limit.

H. Transient Results

As discussed in a previous section, the presence of inorganic oxides, sulfides, and sulfates in the char will affect the composition of the gas in contact with the char. The increase or reduction of the sulfur pressure of the gas in the char will be temporary, since only a finite amount of reactant is introduced with the char. Below a simple model of the transient behavior of char containing calcium oxide and calcium sulfide is developed. This model can easily be extended to include other inorganic compounds.

At the char-gas interface hydrogen sulfide diffuses into the char and reacts with the calcium oxide to form calcium sulfide and water. Close to the char-metal interface, calcium sulfide reacts with water to form calcium oxide and hydrogen sulfide, which diffuses through the char to the metal surface where it reacts.

Penetration Model. The approach described below is based on penetration theory. Two simplifying assumptions are necessary. First, the reaction between the gas phase and the ash (calcium oxide and calcium sulfide in this case) is very fast. This implies that a precisely defined front of ash which has been completely sulfidized will

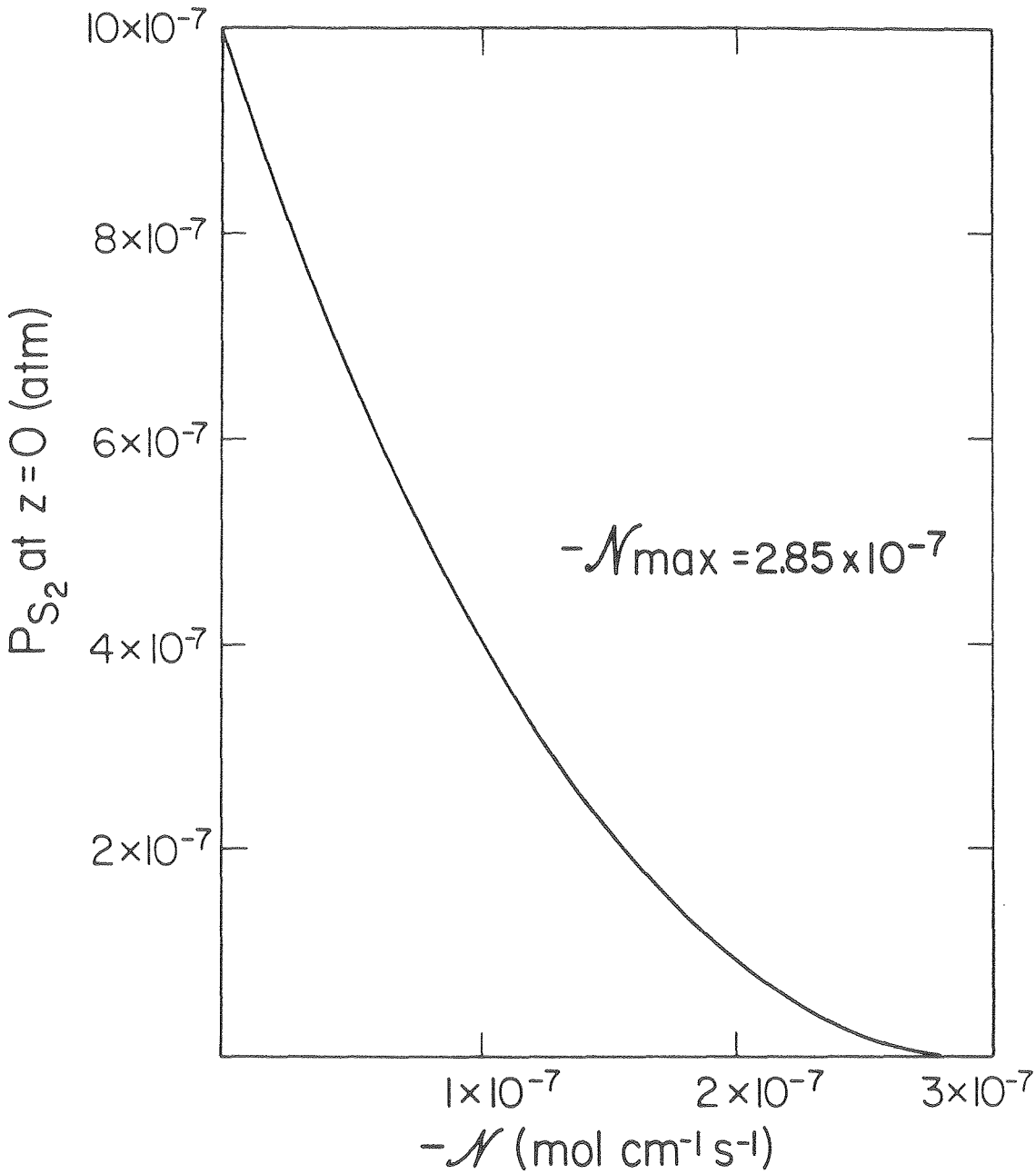

XBL 795-1690

Figure 13. Sulfur Partial Pressure at the Char-Metal Interface vs. Hydrogen Sulfide Flux

move from the char-gas interface into the char. Similarly, a front of completely oxidized ash will move from the char-metal interface into the char. If one also assumes that the transient term, $\varepsilon c \frac{\partial y}{\partial t}$, in the mole balance,

$$\varepsilon c \frac{\partial y_i}{\partial t} + \nabla \cdot N_i = R_i$$

is negligible, the steady state results presented in the previous sections can be used to predict the rate at which the regions which contain no calcium oxide or no calcium sulfide penetrate into the char.

First consider the char-gas interface. The penetration of the reaction front into the char is proportional to the flux of hydrogen sulfide into the char

$$N_{H_2S} = c_o \frac{d}{dt} (L_G) \tag{13}$$

where L_G is the distance of the reaction front from the char-gas interface and c_o is the concentration of calcium oxide in the char (mol cm^{-3}). From the previous discussion we have

$$N = N/L_G \tag{14}$$

N is fixed, since the concentrations at the char-gas interface are fixed, and the composition at L_G is determined by the calcium oxide/calcium sulfide equilibrium. If Equation 14 is substituted into Equation 13, and the resulting differential equation is solved subject to the initial condition that at t=0, L_G=0, one obtains

$$L_G^2 = \frac{N_G}{2c_o} t \tag{15}$$

A similar result is obtained at the char-metal interface. If the rate of sulfidation is mass-transfer limited

$$L_M^2 = \frac{N_M}{2c_s} t \tag{16}$$

In this case L_M is the distance of the reaction from the char-metal interface, and c_s is the concentration of calcium sulfide in the char (mol cm^{-3}). At the char-metal interface, N_M is determined by the calcium oxide/calcium sulfide equilibrium and the fact that the hydrogen sulfide concentration at the metal surface equals zero at the mass-transfer limit. For parabolic kinetics a similar equation can be derived.

Parabolic kinetics imply

$$(\Delta W)^2 = k_p t \tag{17}$$

Differentiating with respect to time, t, yields

$$\frac{dW}{dt} = \frac{k_p}{2\Delta W} \tag{18}$$

Substituting Equation 17 to eliminate Δw yields

$$\frac{dW}{dt} = \left(\frac{k_p}{4t}\right)^{1/2} \tag{19}$$

Since $\frac{dW}{dt}$ equals the mass flux into the scale, Equation 19 can be rewritten as

$$N = \left(\frac{k_p'}{4t}\right)^{1/2} \tag{20}$$

where $k_p' = k_p/(M_S)^2$. Using an expression for N analagous to Equation 13 and rearranging yields

$$dL_M = \frac{\sqrt{k_p'}}{2c_s} t^{-1/2} dt \tag{21}$$

Therefore,

$$L_M^2 = \frac{k_p'}{c_s^2} t \qquad (22)$$

Note that in this case L_M^2 is inversely proportional to the square of the calcium sulfide concentration.

Consider a layer of char 5 cm thick. The char will be assumed to consist of carbon, calcium oxide (0.025 mol/g char), and calcium sulfide (0.04 mol/g char). The calcium oxide and calcium sulfide concentrations are similar to those of Synthane char. A char density of 2 g cm^{-3} is assumed.

Further assume that the oxygen and sulfur partial pressures of the bulk gas are 10^{-20} and 10^{-8} atm, respectively. The calcium oxide/calcium sulfide equilibrium sulfur partial pressure for an oxygen partial pressure of 10^{-20} atm is 1.26×10^{-12} atm. Under these conditions the calculated N_G and N_M are 1.26×10^{-8} mol cm^{-1} s^{-1} and 1.77×10^{-10} mol cm^{-1} s^{-1}, respectively.

Since the penetration at the char-gas interface is much faster than the penetration at the char metal interface, the latter will be ignored. Under the conditions described above, a 5 cm thick layer of char will be completely sulfidized after 2300 days. During this time very little sulfidation of the alloy will occur.

The above results predict that a layer of char which does not react with the sulfur-containing species in the gas phase can nevertheless significantly affect the rate of sulfidation, by limiting the flux of hydrogen sulfide to the metal surface. In many cases, the mass-transfer limit is less than the fluxes predicted by parabolic kinetics. The mass-transfer limited flux is inversely proportional to the thickness of the char layer and approximately directly proportional to the concentration of hydrogen sulfide in the bulk gas. At fluxes up to 80% of the mass-transfer limit the sulfur partial pressure at the char-metal interface differs from the sulfur partial pressure of the bulk gas by less than a factor of ten.

If the char contains ash consisting of inorganic oxides, which react with the sulfur-containing species in the gas phase, the sulfur partial pressure of the gas in the char is determined by the thermodynamics of the reactions between the ash and the gas phase. For elements such as calcium, whose oxides and sulfides are stable at very low oxygen and sulfur partial pressures, the sulfur partial pressure of the gas in the char is usually lower than the sulfur partial pressure in the bulk gas. Under these conditions the flux of hydrogen sulfide to the metal surface is usually less than the flux in the absence of ash, and very little sulfidation is expected as long as the ash has not been completely sulfidized.

CHAPTER 3: EXPERIMENTS

In addition to modelling the effect of coal char on corrosion, experiments demonstrating the effect of coal char on corrosion in coal gasifiers were carried out. Sample coupons of 304 stainless steel were exposed to coal char or graphite in oxidizing or oxidizing/sulfidizing gases at 1200 K. The composition and morphology of the scales formed were analyzed to determine their dependence on the experimental conditions.

A. Apparatus

The experiments were carried out in the vertical tube furnace pictured in Figures 14 and 15. Note that three isolated samples can be exposed simultaneously. Gas enters and leaves through the upper section. The flow rate of the entering gas is set with a flow meter--usually at 20 cm^3/min. After the sample coupons and char are placed into the ceramic tubes, these are attached to the upper section, and the entire assembly is lowered into the hot zone of the furnace. The temperature in the hot zone is controlled within ± 3 K. Because of the low mass of the tubes, only about 10 minutes are required to return to the set temperature after the tubes are lowered. Natural convection, due to the temperature difference between the upper section which remains exposed to the room and the lower half of the tubes in the hot zone, ensures that the gas entering the apparatus is thoroughly mixed with the gas above the char.

Some experiments were carried out in a closed environment, with no gas flow in or out of the apparatus. This eliminated effects due to the composition of the covering gas and prevented any loss by convection of the reactive species formed from the char. Since this apparatus cannot

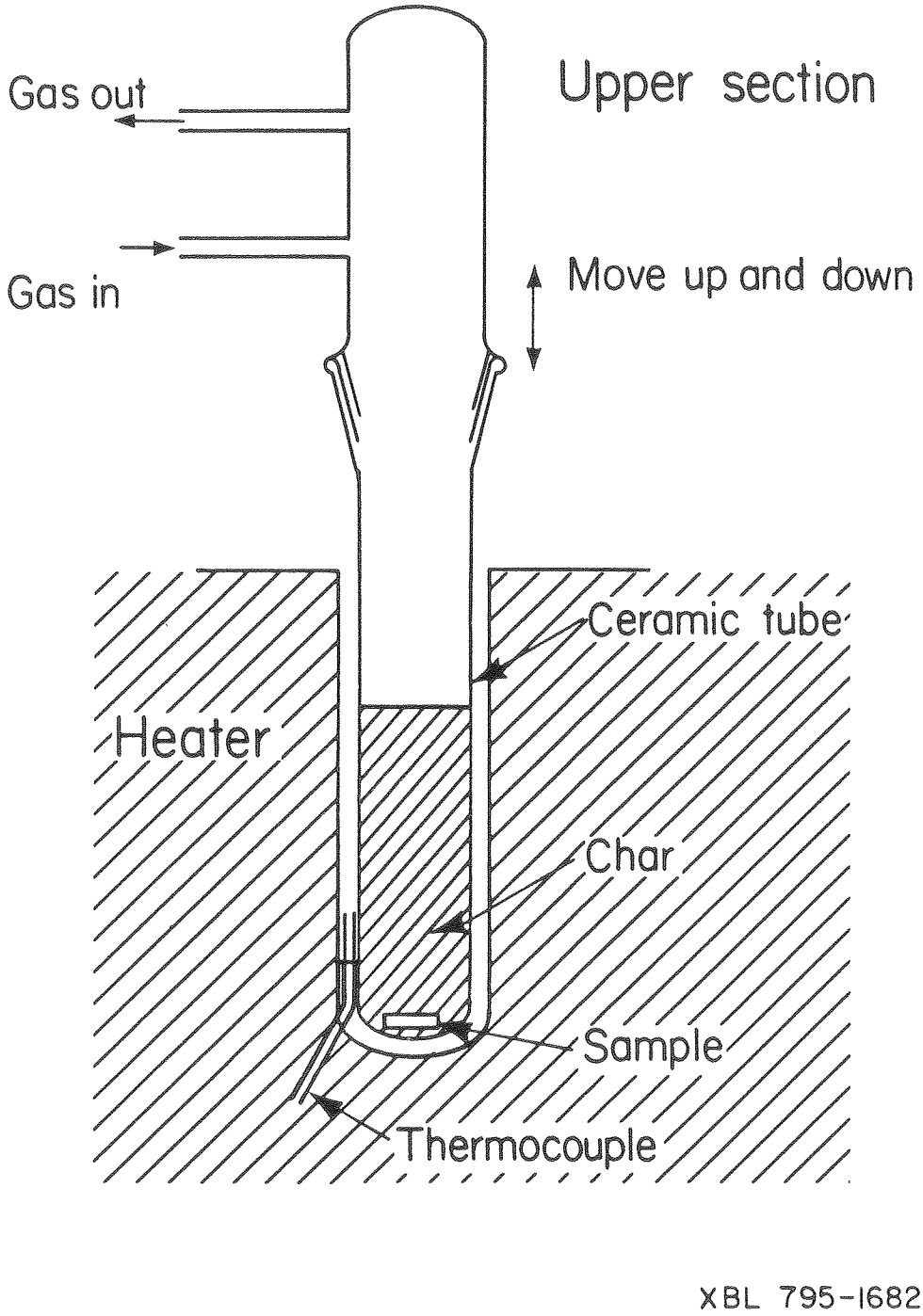

Figure 14. Diagram of Experimental Apparatus

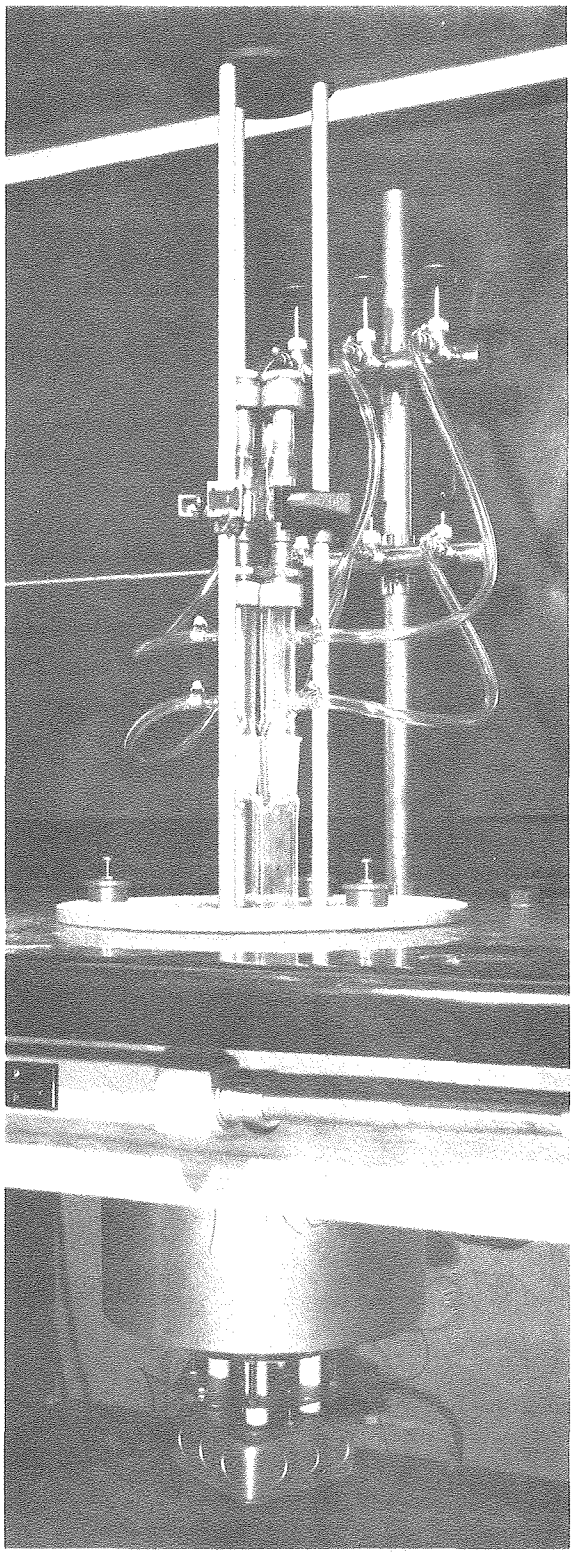

XBB 781-776

Figure 15. Photograph of the Experimental Apparatus

be pressurized far above atmospheric pressure because of the joint between the upper section and the ceramic tubes, the system was evacuated before the tubes were inserted into the furnace. This ensured that despite the pressure rise in the tubes due to the temperature rise, the pressure in the tubes did not rise above atmospheric pressure.

B. Experimental Procedure

The 304 SS sample coupons were cut from a piece of 2 mm thick sheet metal and polished through 600 grit with silicon carbide paper, washed with ethanol and acetone, air dried, and weighed.

The samples were usually exposed for 24 hours. Upon conclusion of an experiment, char which loosely adhered to the surface of the exposed samples was brushed off, and the samples were weighed again, and the weight gain was recorded. The samples were then mounted with phenolic strips in Bakelite. Klarmount was used around the edges to improve edge retention during the subsequent polishing. The mounted samples were cross sectioned by removing a layer of mounting material and the sample with 320 and 600 grit silicon carbide papers. The exposed cross sections were then polished for 4 to 6 hours with 1 micron diamond paste on a nylon cloth. The final polish was carried out with a Leco 0.05 micron abrasive suspension in water.

The morphology and composition of the corrosion products were studied by scanning electron microscopy (SEM) and energy dispersive x-ray analysis (EDAX).

C. Experiments

Three chars--FMC, HUSKY, and Synthane char--were used in these experiments. The compositions of these chars are listed in Tables II

and VII. All three chars were formed in laboratory and pilot plant runs performed elsewhere. FMC char was formed from Western Kentucky coal by the FMC-CoEd process. The Husky char was formed from North Dakota Lignite and the Synthane char from Illinois #6 coal.

The char analyses were carried out by completely oxidizing a sample of char. Therefore, it is impossible to determine the original species in the char. Some deductions about the original compositions can be made. For example, 1 g FMC char contains 0.084 mol sulfur. However, 0.15 g ash (the amount in 1 g FMC char) contains only 0.0073 mol sulfur. It also contains 0.0099 mol calcium. This implies that most of the sulfur is not in the ash, but in the volatile matter. There is not enough calcium in the ash to react with all of the sulfur in the char as described in Chapter 2.

A similar analysis can be carried out for the Husky char. The char contains 0.028 mol sulfur per gram of char. Calculations show that the ash contains 0.0315 mol sulfur and 0.053 mol calcium. The small discrepancy in the sulfur content of the char and the ash is probably due to experimental errors. For Husky char, all of the sulfur is in the ash, which contains enough calcium to react with all of the sulfur in the char to form calcium sulfide. Calcium sulfate would not be formed since it is unstable at the low oxygen pressures in coal char. Presumably the remaining calcium is calcium oxide. The excess calcium oxide in Husky char, defined as the difference between the mol calcium and mol sulfur per gram of char, is 0.021 mol calcium oxide per gram of char.

The excess calcium oxide of Synthane char is 0.027 mol calcium oxide per gram char (assuming that Synthane char consists of 55% ash).

Table VII: Compositions of FMC and Husky Chars*

	FMC (W. Kentucky Colonial Mine, High-Volatile B Bituminous)	Husky (N. Dakota Lignite)
Proximate Analysis, w/o dry		
Volatile Matter	3.5	7.7
Fixed Carbon	81.5	69.2
Ash	15.0	23.1
Ultimate Analysis, w/o dry		
Carbon	75.0	72.3
Hydrogen	1.7	1.6
Nitrogen	1.5	0.9
Sulfur	2.7	0.9
Oxygen	4.1	1.2
Ash	15.0	23.1
Ash Analysis, w/o dry		
SiO_2	47.8	40.7
Al_2O_3	14.0	9.1
Fe_2O_3	24.1	11.5
CaO	3.7	12.7
MgO	0.2	8.7
K_2O	1.3	1.8
Na_2O	4.0	4.0
SO_3	3.9	10.9
TiO_2	0.9	0.6

*From Ref. 12

Experiments using graphite with sulfidizing/oxidizing gases were also carried out.

Two premixed sulfidizing gases were employed. Mixture A contained 3.5% H_2, 1% H_2S, and the balance consisted of CO_2. Mixture B contained 4% H_2, 0.01% H_2S, and the balance consisted of CO_2. At 1200 K, the approximate sulfur partial pressures of mixtures A and B are 10^{-4} and 10^{-8} atm, respectively. The nonsulfidizing mixture (C) consisted of 37% CO_2 and 63% CO. This mixture has an oxygen partial pressure of about 10^{-15} atm at 1200 K. In the char the CO_2 in the gases will be reduced to CO and the oxygen partial pressure will be determined by the C/CO equilibrium ($p_{O_2} < 10^{-18}$ atm).

The experimental conditions for each run are listed in Table VIII. The measured weight gains are recorded there also.

D. Corrosion in Sulfur-Free Bulk Gases

The extent of corrosion is often measured as the weight gain per unit surface area. For the expeirments discussed below the weight gains are not an accurate measure of the extent of corrosion. Only the total weight gains were measured. All of the samples were approximately the same size, but the exact surface areas were not recorded. Two other factors further reduce the accuracy of these measurements. Scale is lost through spalling during cooling of the samples, and the measured apparent weight gains are too high because char particles become embedded in the scale. Because of these limitations, only qualitative comparisons should be based on the weight gains recorded in Table VIIIand Figures 16 and 17.

Most of the analysis below is based on comparisons of cross sections which indicate the thickness of the scales formed, and how far internal attack has penetrated the sample.

Table VIII: List of Experiments

run	bulk gas*	char	time (hrs.)	weight gain (mg)
1	open	10 g FMC	24	67.6
2	"	10 g Husky	"	4.5
3	"	10 g Synthane	"	10.3
4	closed	10 g FMC	"	130.4
5	"	10 g Husky	"	3.4
6	"	10 g Synthane	"	8.0
7	"	10 g FMC	48	153.9
8	"	10 g Husky	"	6.7
9	"	10 g Synthane	"	13.2
10	C	10 g FMC	24	30.9
11	"	10 g Husky	"	3.3
12	"	10 g Synthane	"	6.3
13	A	no char	"	7.2
14	"	5 g FMC	"	28.2
15	"	10 g FMC	"	33.6
16	"	no char	"	-4.5
17	"	depl. char from 14	"	4.1
18	"	depl. char from 15	"	4.8
19	"	no char	"	1.0
20	"	5 g Synthane	"	12.1
21	"	10 g Synthane	"	11.6
22	"	no char	"	9.7
23	"	5 g graphite	"	16.6
24	"	10 g graphite	"	6.6
25	"	0.5 g Synthane	"	5.2
26	"	5 g Synthane	"	8.9
27	"	10 g Synthane	"	6.5
28	"	10 g FMC	96	63.4
29	"	10 g Synthane	"	17.5
30	"	10 g graphite	"	3.1
31	B	10 g graphite 24	24	3.7
32	"	10 g FMC	"	18.4
33	"	10 g Synthane	"	6.9

*open = system flushed with C and then closed inlet valve
closed = system flushed with C, closed, and then evacuated
A = 20 cm^3/min of 1% H_2, 3.5% H_2S, balance CO_2
B = 20 cm^3/min of 0.01% H_2, 3.5% H_2S, balance CO_2
C = 20 cm^3/min of 63% CO_2, 37% CO

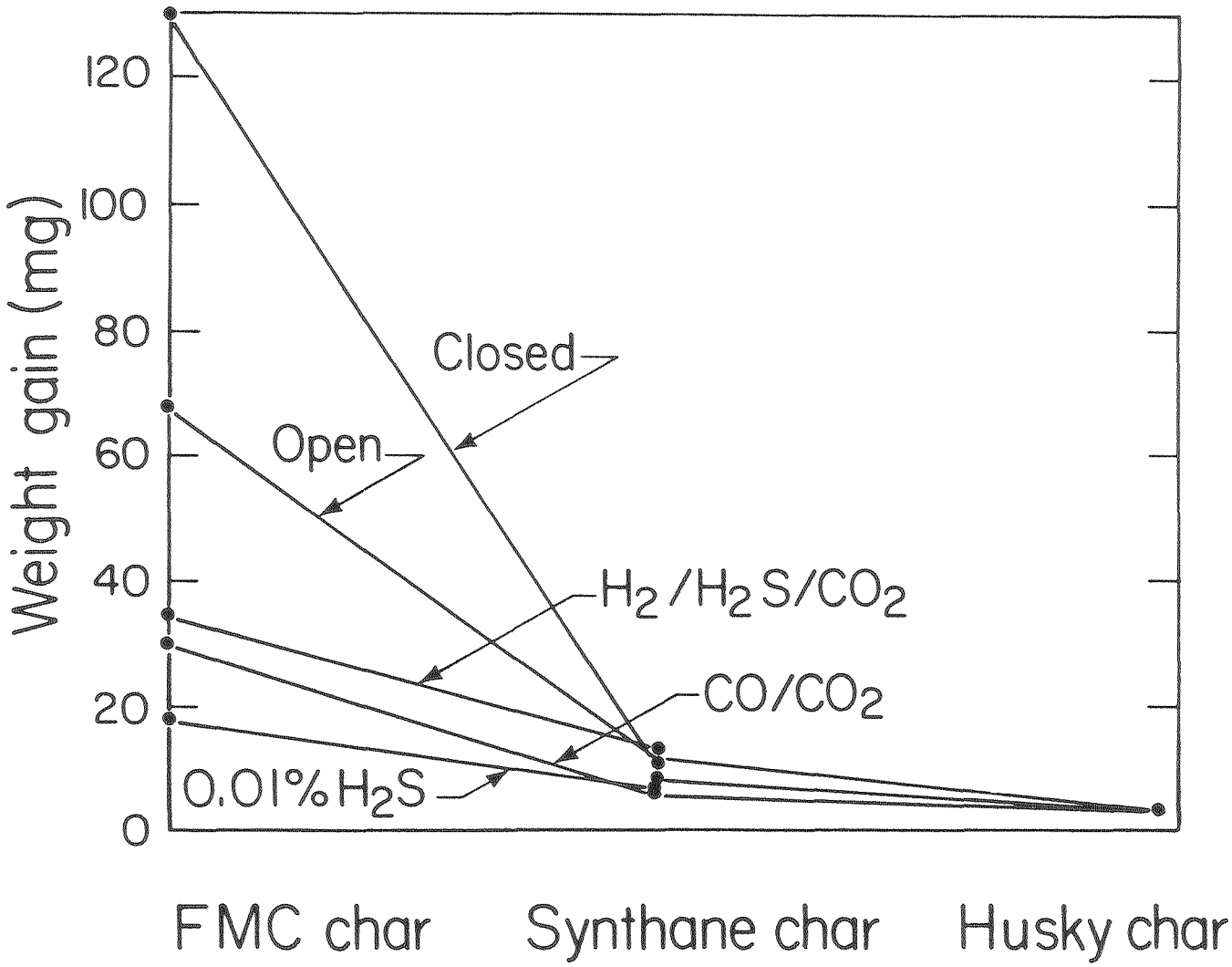

XBL 795-1670

Figure 16. Summary of Weight Gains Demonstrating the Effect of Coal-Char Composition

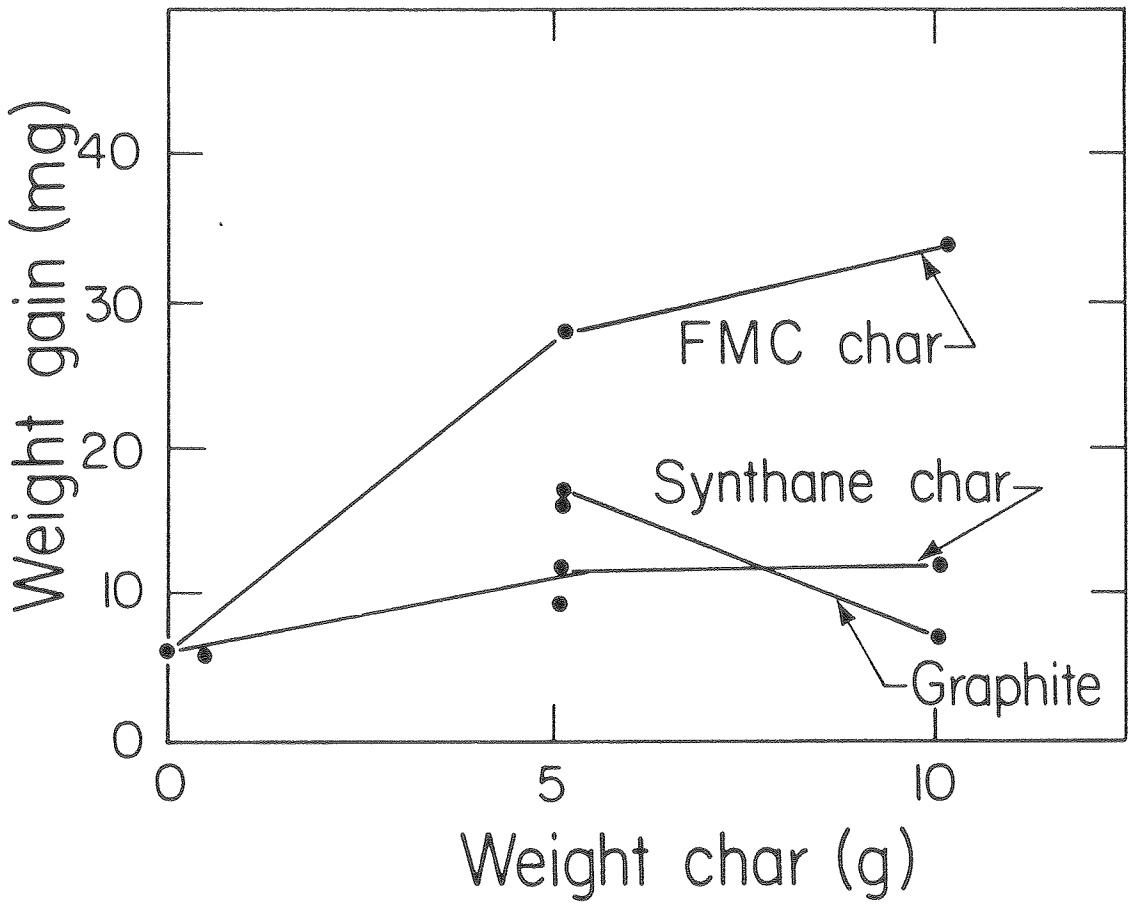

XBL 795-1668

Figure 17. Summary of Weight Gains Demonstrating the Effect of Coal-Char Quantity.

Effect of char composition. Runs 1 through 12 clearly show that in sulfur-free bulk gases FMC char is much more sulfidizing than Husky or Synthane char. This is demonstrated by the measured weight gains and by SEM and EDAX analysis of cross sections of the samples. Under all conditions a thick external sulfide scale is formed on samples exposed to FMC char. Extensive internal attack occurs also. Only internal sulfidation occurs in samples exposed to Husky or Synthane char.

Cross sections of the samples from runs 4,5, and 6 (closed environment) are shown in Figures 18 through 21. In these and all subsequent figures of sample cross sections, the mounting material is on the left, and the unreacted bulk metal is on the right of the photographs. Figure 18 shows that char particles are embedded in the external sulfide scale formed on samples exposed to FMC char. EDAX analysis of the scale reveals that it contains iron, chromium, and sulfur. Only one phase is visible at high magnifications (10,000X) which implies that the scale is a mixed iron-chromium sulfide. The light region immediately below the scale consists of iron and nickel, and is free of chromium and sulfur. The region of internal attack consists of at least three phases (see Figures 18 and 19). Element maps of the region in Figure 19 show that the light phase again consists of iron and nickel, but is depleted of chromium. It contains little or no sulfur. The grey phase consists of iron, chromium, and sulfur. Again, only one phase is visible. The light regions were probably formed by the diffusion of chromium into the grey regions where the chromium reacted to form sulfides. The black regions are silicon rich and free of sulfur. They are probably silicon oxide. Small quantities of

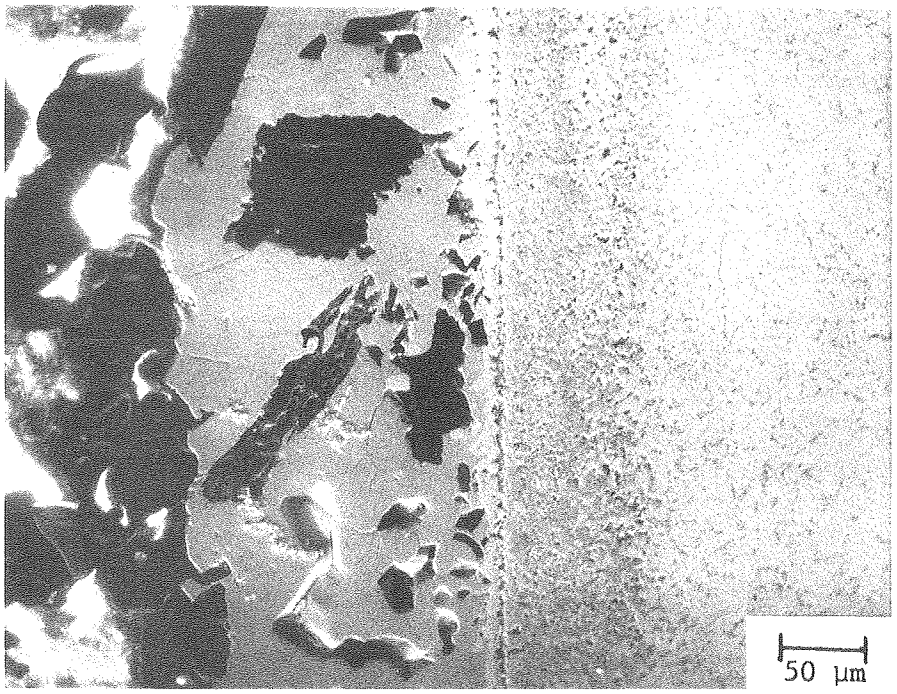

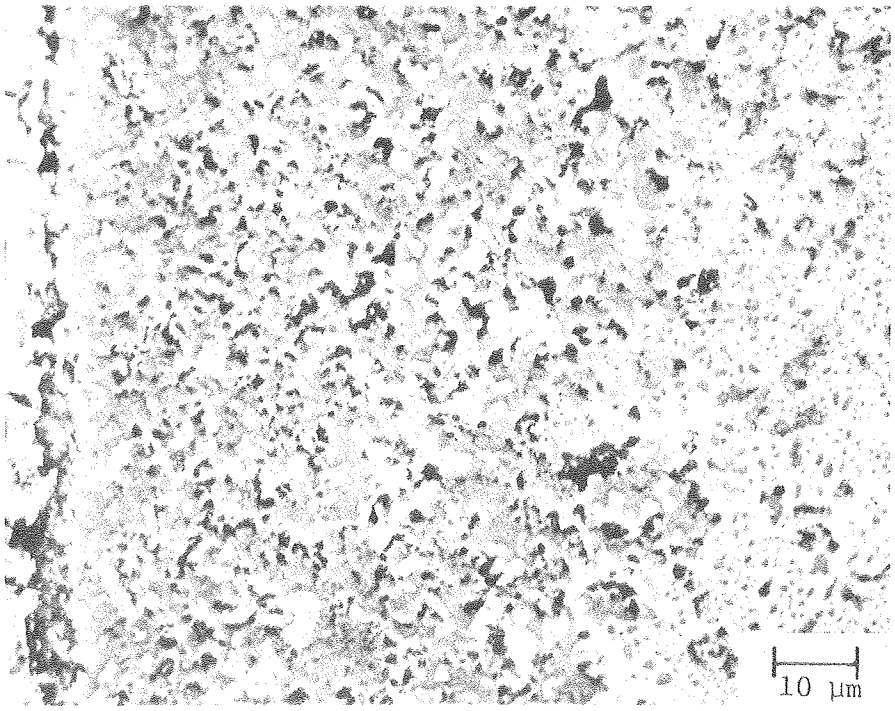

XBB 795-6632

Figure 18. Cross Sections of a Sample Exposed to FMC Char for 24 hours in a Closed Environment.

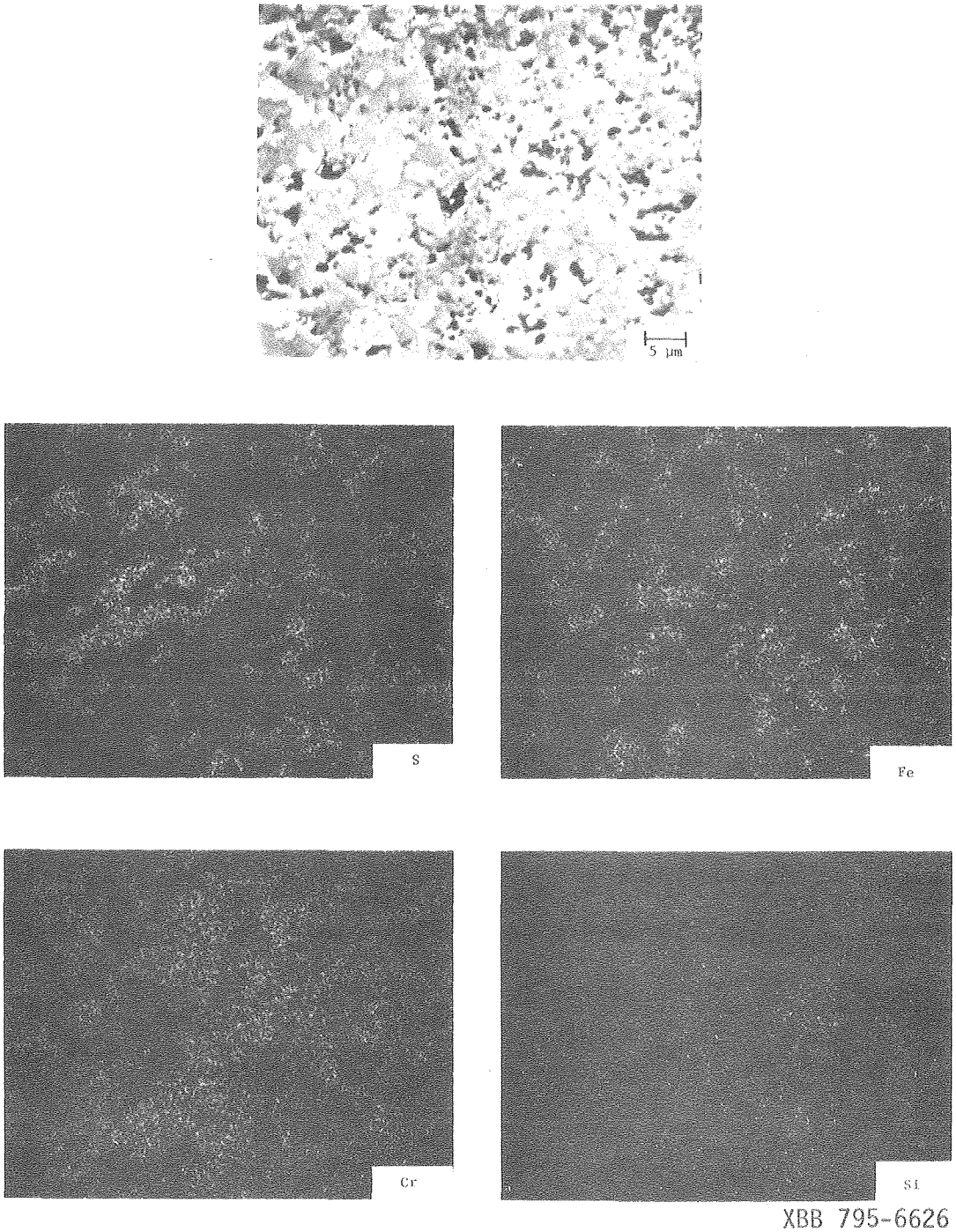

Figure 19. Cross Section of the Internal Attack of a Sample Exposed to FMC Char for 24 hours in a Closed Environment

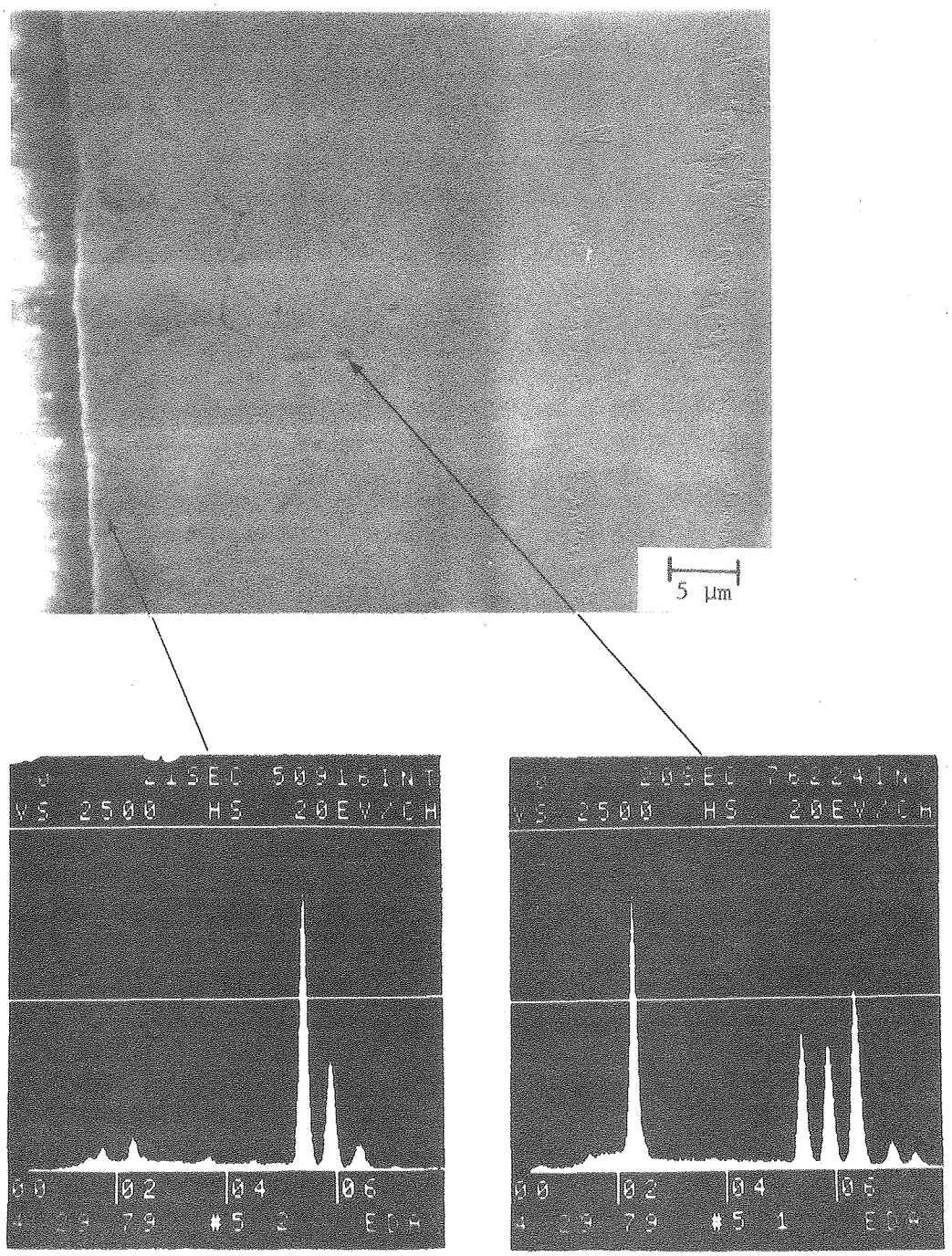

XBB 759-6629

Figure 20. Cross Section of a Sample Exposed to Husky Char for 24 hours in a Closed Environment

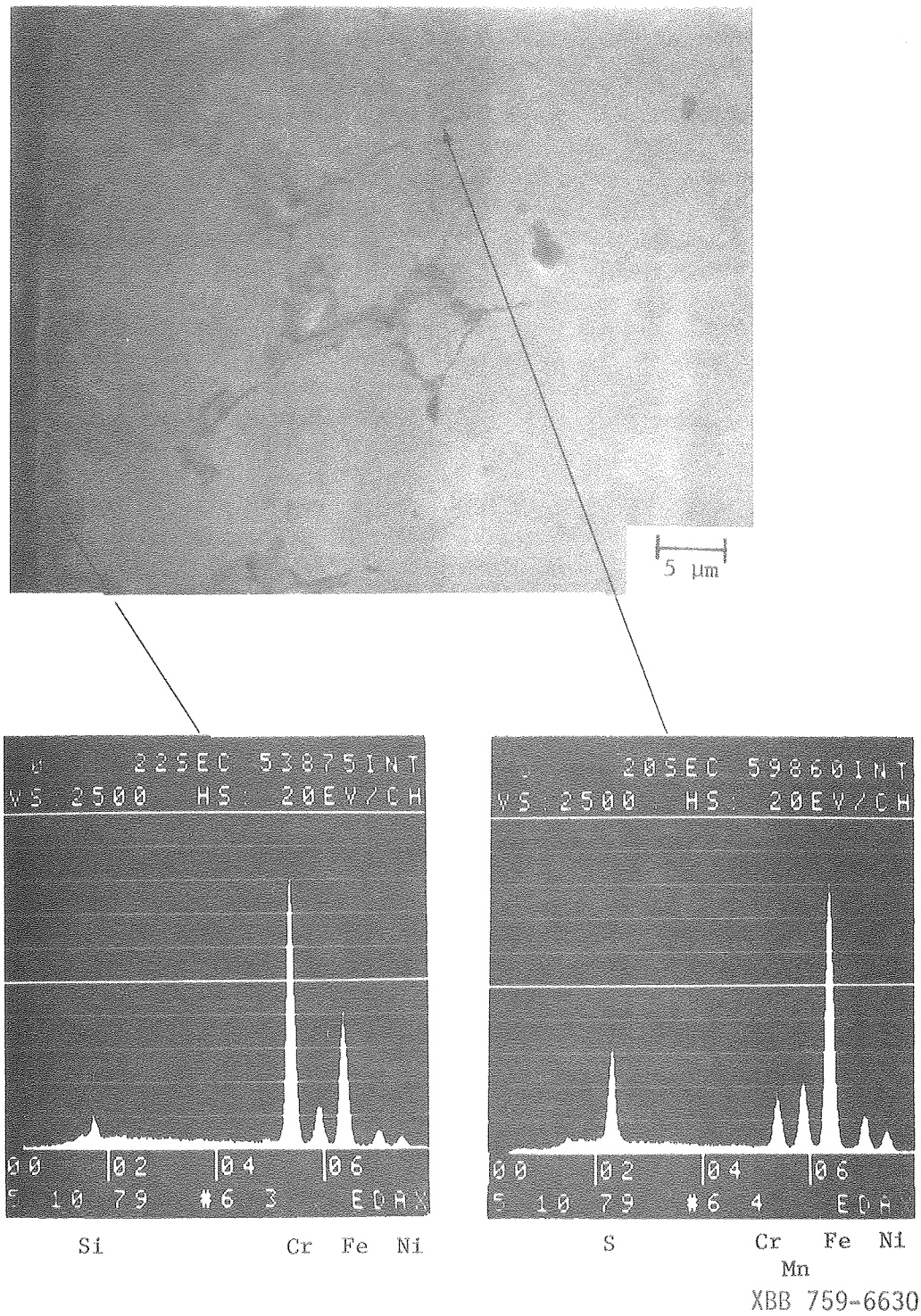

Figure 21. Cross Section of a Sample Exposed to Synthane Char for 24 hours in a Closed Environment

silicon are usually added to commercial steels as an oxygen getter.

The cross sections of samples exposed to Husky and Synthane chars are very similar to each other (Figures 20 and 21, respectively). The grey regions at the surface, which penetrate into the metal along grain boundaries, are rich in chromium and free of sulfur. They are probably chromium oxide. The round and oval grey inclusions are sulfides. The metallic elements present in the sulfides include iron chromium, and manganese. The sulfides lie along grain boundaries close to the metal surface. They are not observed in the unreacted bulk alloy.

Manganese is usually added to metals to react with sulfur during the production of the steel. The fact that these sulfides are only observed close to the surface and not in the bulk alloy, implies that these sulfides were formed during these experiments and not during the production of the steel.

The very dark elongated regions along grain boundaries are silicon oxide.

Exposure time. Increased weight gains are measured for all three chars if the exposure time in the closed environment is increased from 24 to 48 hours. However, the cross sections of samples exposed to Husky and Synthane char in a closed environment for 24 or 48 hours do not differ greatly. The corrosion is limited to oxidation along grain boundaries and the formation of internal sulfides. Slightly thicker sulfide scales form on samples exposed to FMC char in a closed system for 48 hours than on samples exposed for 24 hours. The pattern of attack is unchanged.

Convective Effects. If the experiments are carried out in an open system, with gas flow in or out of the apparatus, the extent of

corrosion of samples exposed to FMC char decreases. The weight gain of samples exposed to FMC char with no flow of bulk gas into the system and the outlet valves open, (run 1), is less than the weight gain of samples exposed in a closed environment (run 4). The weight gain decreases further if there is a flow of the bulk gas in and out of the apparatus (run 10). The cross sections also clearly demonstrate this trend (Figures 18 and 22a). The pattern of attack--an outer sulfide scale, and a region of extensive internal attack immediately below it--is unchanged. The same pattern is observed in all other experiments with FMC char.

The effect of the bulk gas flow on corrosion by Husky and Synthane char is much less. Both the pattern and extent of attack in samples exposed to these chars in mixture C (Figure 22 b,c) do not differ significantly from those of samples exposed to these chars in a closed environment (Figures 20 and 21).

The decrease in attack by FMC char with increasing bulk gas flow is probably due to the loss of the sulfur containing volatiles in the gas flowing out of the apparatus. This reduces the amount of sulfur which can react with the metal. In Synthane and Husky char the sulfur pressure at the metal surface is determined by the calcium oxide/calcium sulfide equilibrium (see Chapter 2) and much smaller effects by the bulk gas flow rate are observed, since the metal does not "see" the gas above the char if the exposure times are short enough.

E. Corrosion in Sulfur Containing Bulk Gases

Effect of char composition. The corrosion of samples exposed to mixture A ($p_{S_2} \sim 10^{-4}$ atm) in the absence of char is not very reproducible. If an adherent chromium oxide scale forms it usually

Figure 22. Cross Sections of Samples Exposed to FMC, Husky, and Synthane Chars for 24 hours in Mixture C

a - (top) FMC char

b - (bottom left) Husky char

c - (bottom right) Synthane char

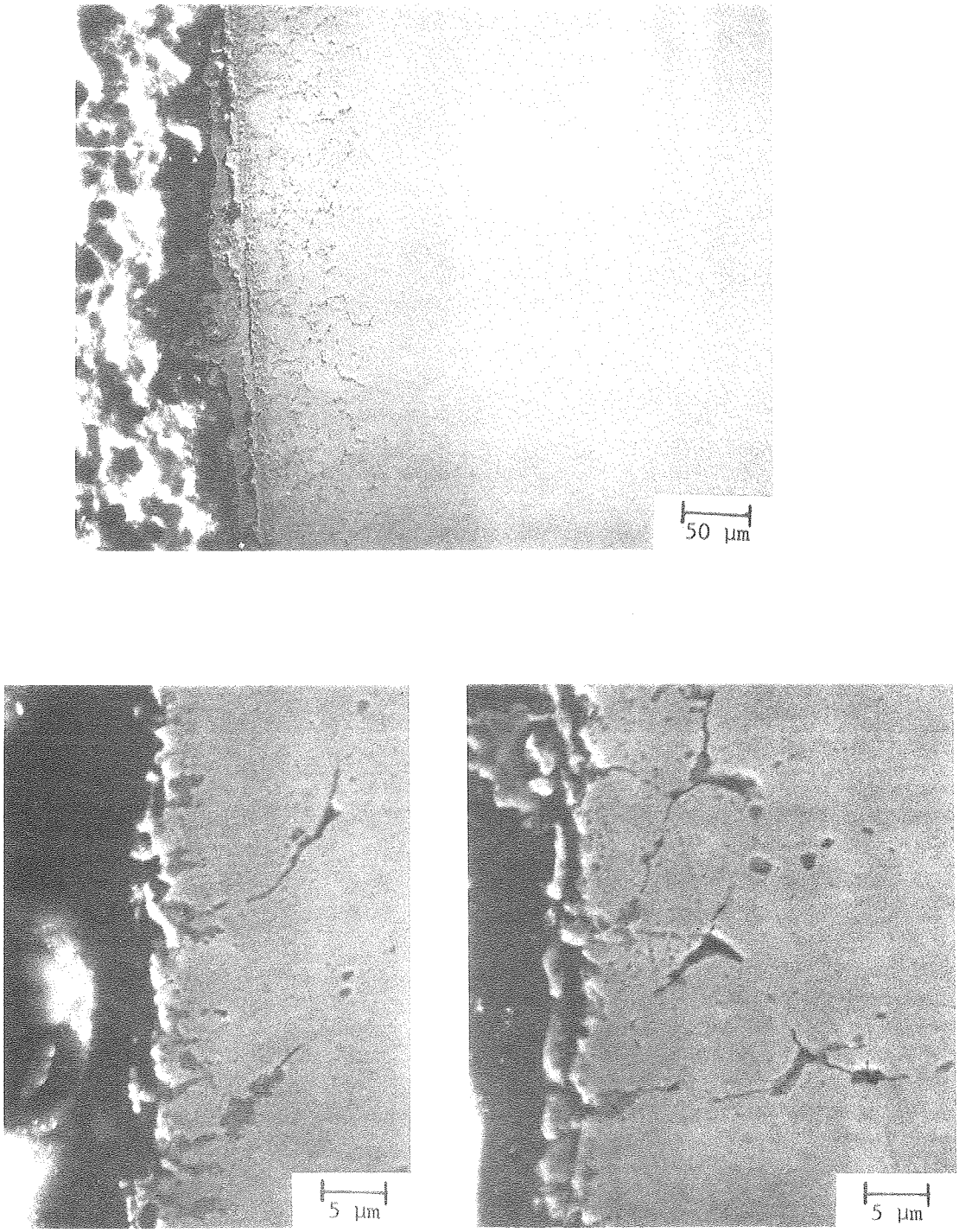

XBB 795-6631

Figure 22

is protective and only small internal sulfides containing manganese, iron, and chromium are observed in the metal below the scale. If a protective oxide layer does not form, extensive internal sulfidation and sulfide scale formation occurs (Figure 23). EDAX analysis of the uniform scale shown in Figure 23a reveals the presence of chromium and small amounts of iron. Presumably this scale is chromium oxide with small amounts of iron oxide. X-ray diffraction to determine if the iron chromium spinel is formed was not carried out. A region of extensive sulfidation is shown in Figure 23b. The grey regions are iron chromium sulfides.

Much less oxidation is observed in the presence of char. This is due to the lower oxygen partial pressure resulting from the presence of carbon. The observed attack depends on the type of char.

The extent and morphology of corrosion of samples exposed for 24 hours in mixture A and FMC or Synthane char do not differ significantly from the corrosion with these chars in the sulfur free bulk gas (compare run 10 with 14 and 15; and 12 with 20, 21, 26, and 27). The measured weight gains under both conditions are similar also. Again FMC char is much more corrosive than Synthane char.

Sulfide scales form on samples exposed to mixture A and graphite (runs 23, 24; Figures 24 and 25). The composition and morphology of the scales changes slightly from one side of the sample to the other. The outer scale is rich in iron and sulfur. On one side (A) it is free of chromium, while the scale on the other side (B) contains some chromium. The scale on side B is more continuous and more adherent than the scale on side A. EDAX analysis does not permit the determination of the ratio of iron to sulfur in the scales. Therefore, it is

Figure 23. Cross Sections of Samples Exposed to Mixture A for 24 hours

a - (top) protective chromium oxide scale

b - (bottom) extensive sulfidation

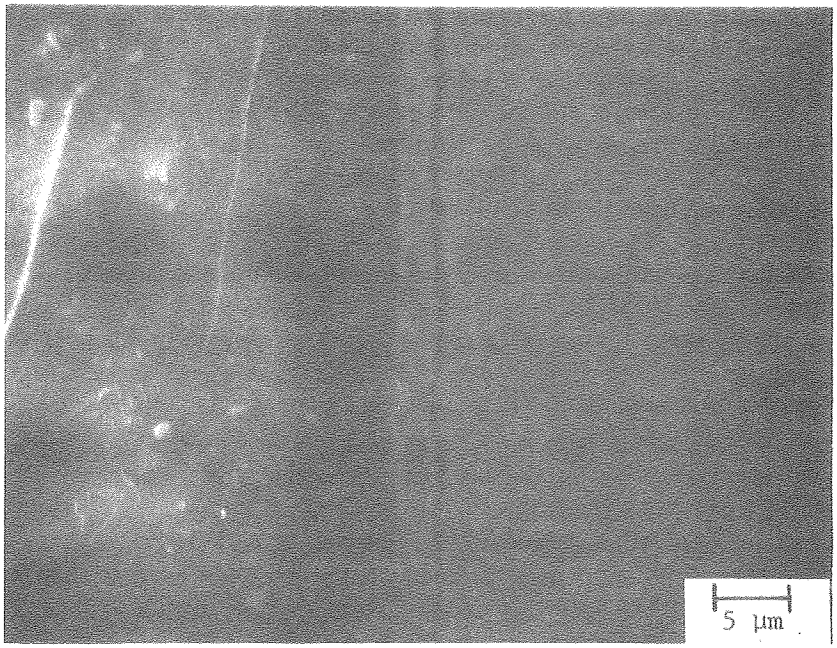

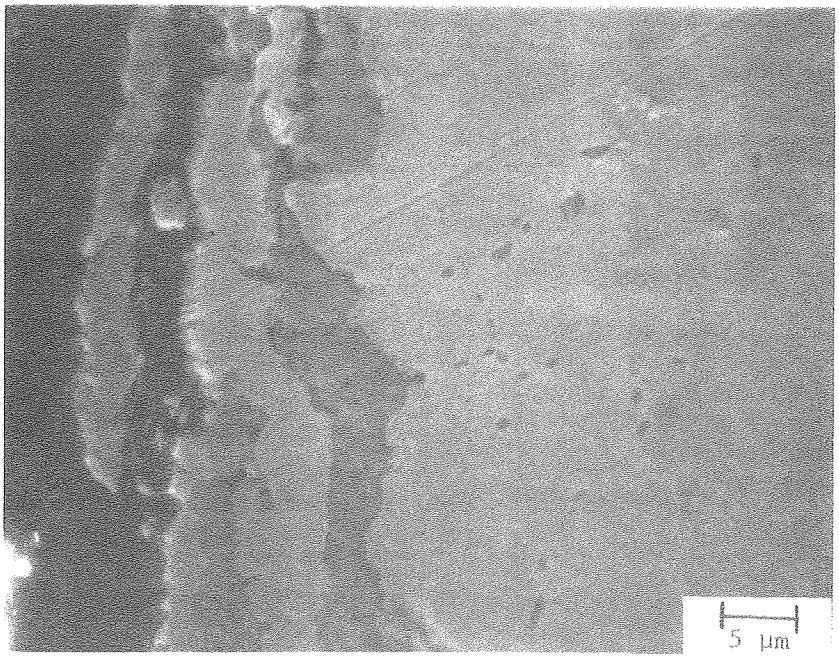

XBB 759-7479

Figure 23

Figure 24. Cross Sections of Sample Exposed to 5 grams Graphite for 24 hours in Mixture A

a - (top) side A

b - (bottom) side B

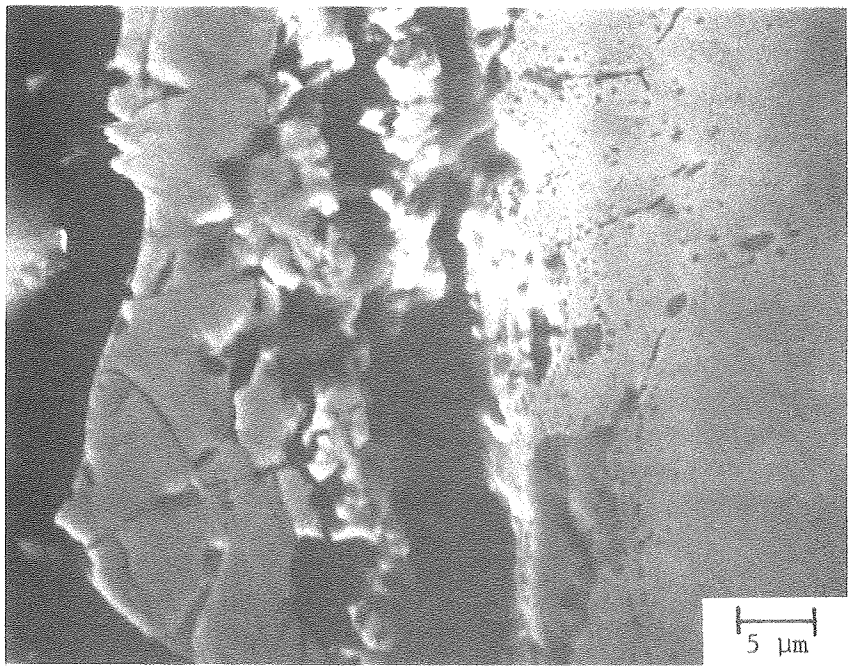

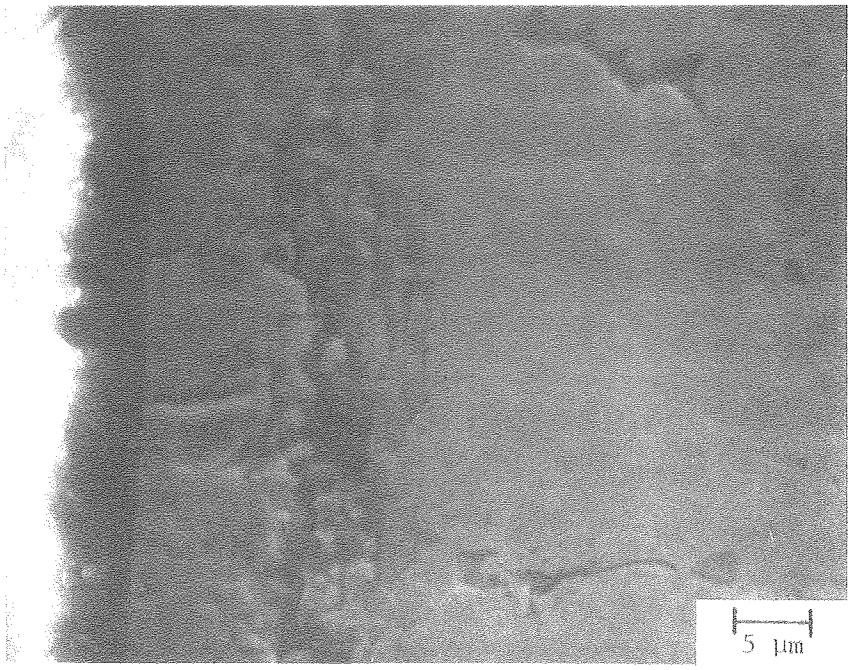

XBB 795-6904

Figure 24

Figure 25. Cross Sections of Sample Exposed to 10 Grams Graphite for 24 hours in Mixture A

a - (top) side A

b - (bottom) side B

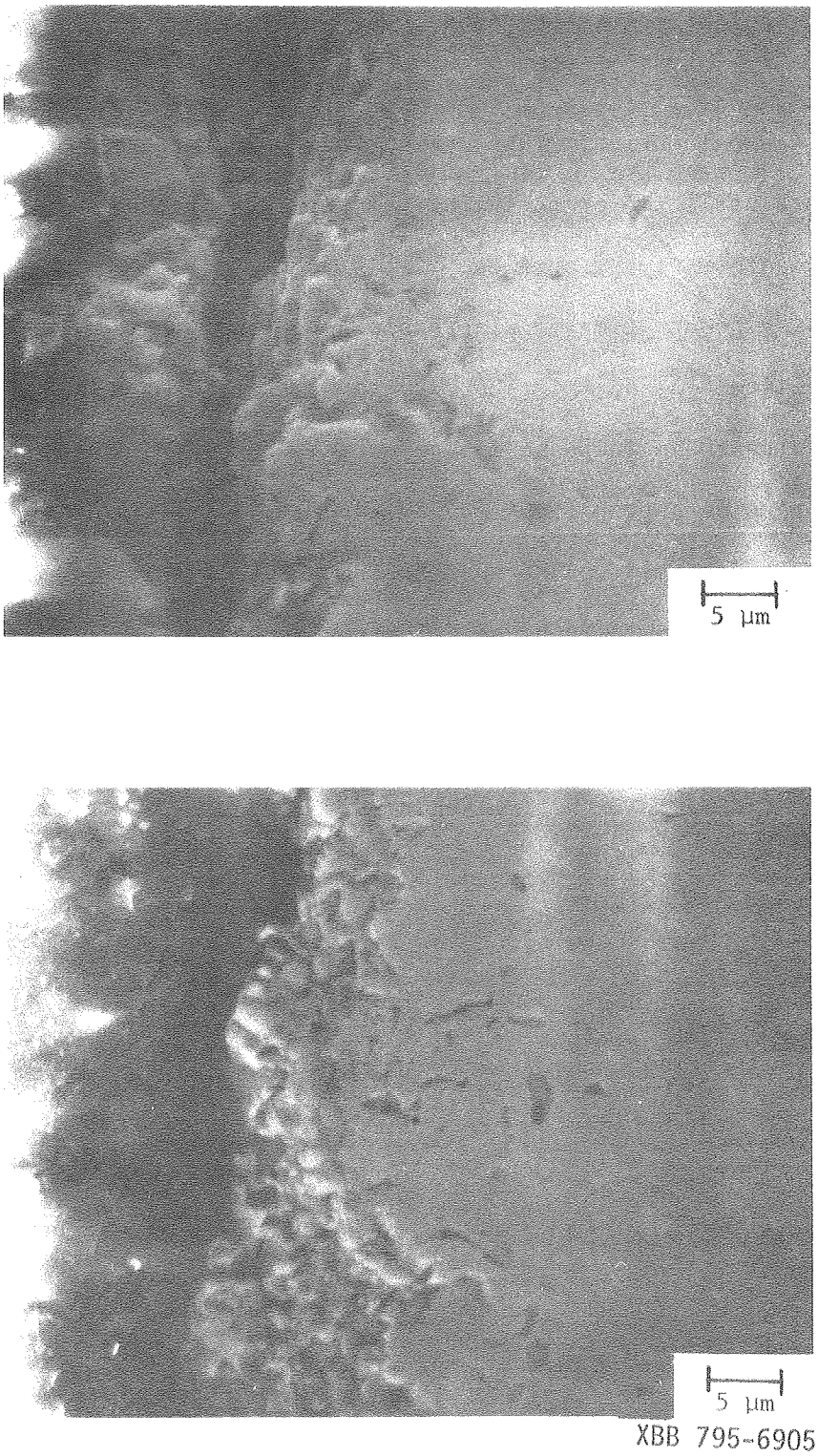

Figure 25

not possible to state if the scale is iron sulfide (FeS) or some other non-stoichiometric compound.

Generally the grey regions immediately below the sulfide scale are chromium rich. This region, which presumably is chromium oxide, contains little or no sulfur. Internal sulfides, rich in manganese, form close to the surface.

Exposure times. Increasing the exposure time of samples exposed to mixture A and FMC char, Synthane char, or graphite to 96 hours results in an increase in the extent of attack, but no change in the pattern of attack (runs 28, 29, and 30). The outer scale formed on samples exposed to FMC char for 96 hours is thicker than on samples exposed for only 24 hours. The region below the outer scale is totally sulfidized. Only one continuous phase is visible (Figure 26). This phase consists of iron, chromium and sulfur. More extensive oxidation at the surface of the sample and along grain boundaries is observed in samples exposed to Synthane char for 96 hours than in samples exposed under the same conditions for 24 hours. Increasing the exposure time from 24 to 96 hours does not lead to increased sulfidation (Figures 27a and 21; note the difference in magnification). Thicker sulfide scales form on samples exposed to graphite for 96 hours than on samples exposed for 24 hours (Figures 27b and 25). No other differences are apparent.

Effect of bulk gas composition. The corrosion of samples in Synthane char and FMC char in mixture B ($p_{S_2} \sim 10^{-8}$ atm) is the same as that observed with mixture A ($p_{S_2} \sim 10^{-4}$ atm) and the sulfur-free mixture (C). With graphite the attack changes from sulfide scale formation to oxide scale formation. Iron oxide scales form on samples

Figure 26. Cross Section of a Sample Exposed to FMC Char for 96 hours in Mixture A

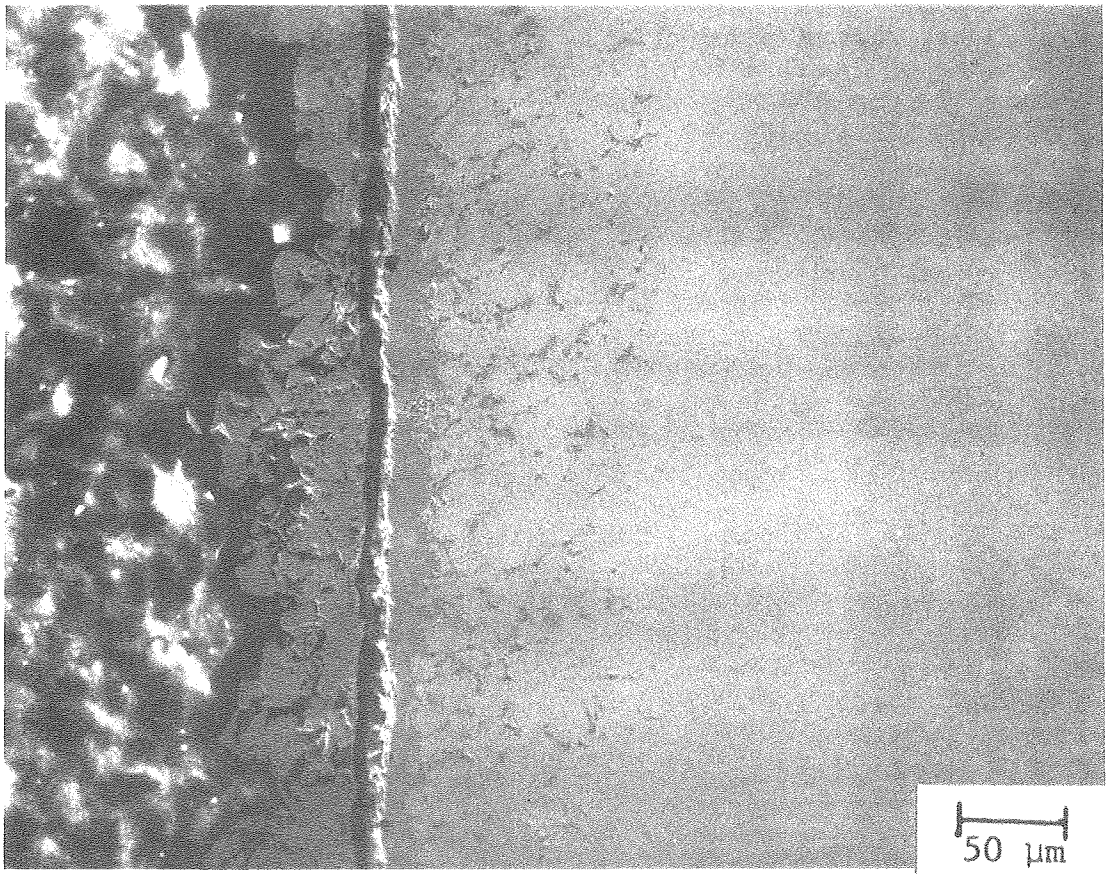

XBB 759-7481

Figure 26

Figure 27. Cross Sections of Samples Exposed to Synthane Char and Graphite for 96 hours in Mixture A

a - (top) Synthane Char

b - (bottom) Graphite

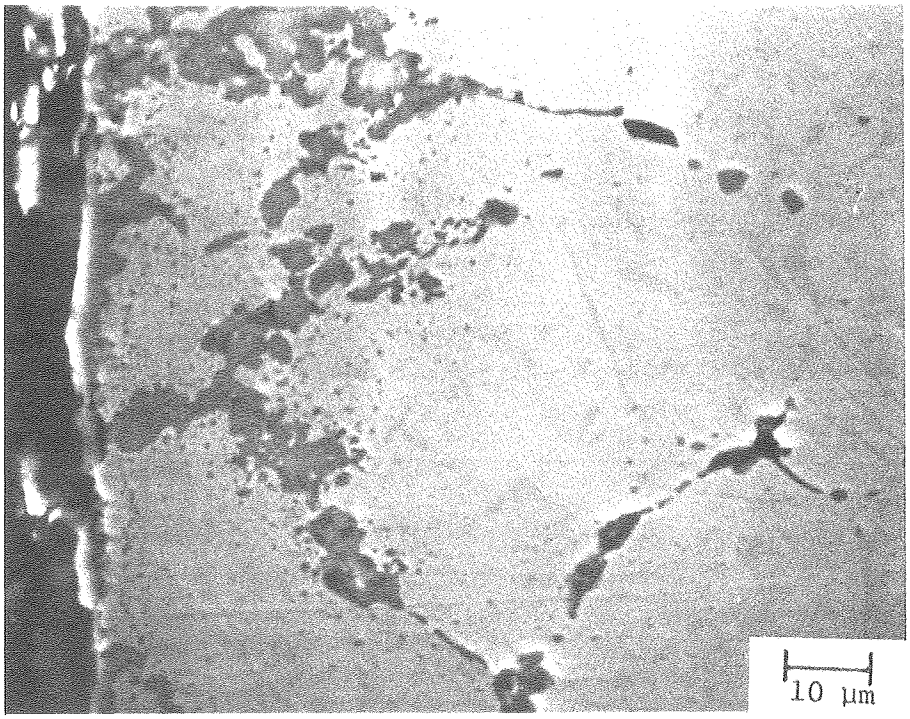

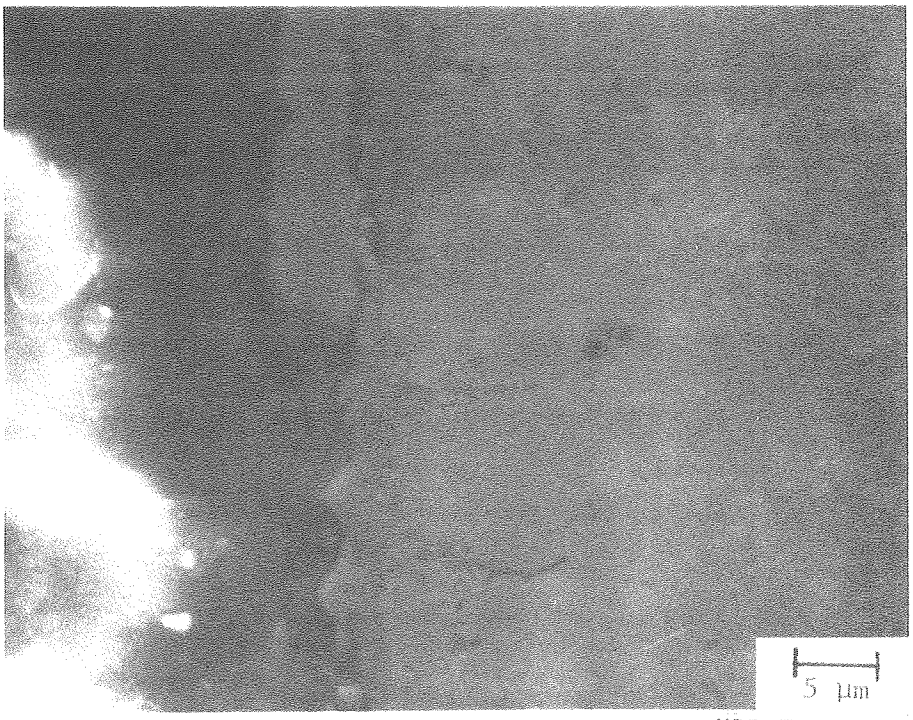

XBB 759-7478

Figure 27

exposed to the low sulfur bulk gas and graphite (Figure 28). Immediately below the scale is a region which consists of iron, chromium, and sulfur. Again only one phase is observed, so this phase probably is a mixed iron chromium sulfide. Small internal sulfides also form.

Char quantity effect. Under some conditions the quantity of char affects the extent of corrosion. Much more oxidation occurs in samples exposed to 0.5 g Synthane char than in samples exposed to 5 g or 10 g char. The outer chromium oxide layer is thicker and internal oxidation along grain boundaries is more extensive in samples exposed to 0.5 g Synthane char (Figure 29) than to 5 g or 10 g Synthane char (Figure 16). Samples exposed to 10 g Synthane char consistently have slightly lower weight gains than samples exposed to 5 g Synthane char. However, no significant difference in the cross sections is observed.

With graphite a char quantity effect is observed also. The weight gain of samples exposed in mixture A to 10 g graphite is less than the weight gain of samples exposed to only 5 g graphite. This decrease in corrosion is also apparent from the cross sections of the samples (Figures 24 and 25). This decrease was predicted by the equations developed in Chapter 2.

The observed corrosion behavior in sulfur containing bulk gases is explained by the compositions of the chars. In the presence of FMC char the composition of the gas in the char is determined by the volatiles which are driven off the char and is independent of the composition of the bulk gas.

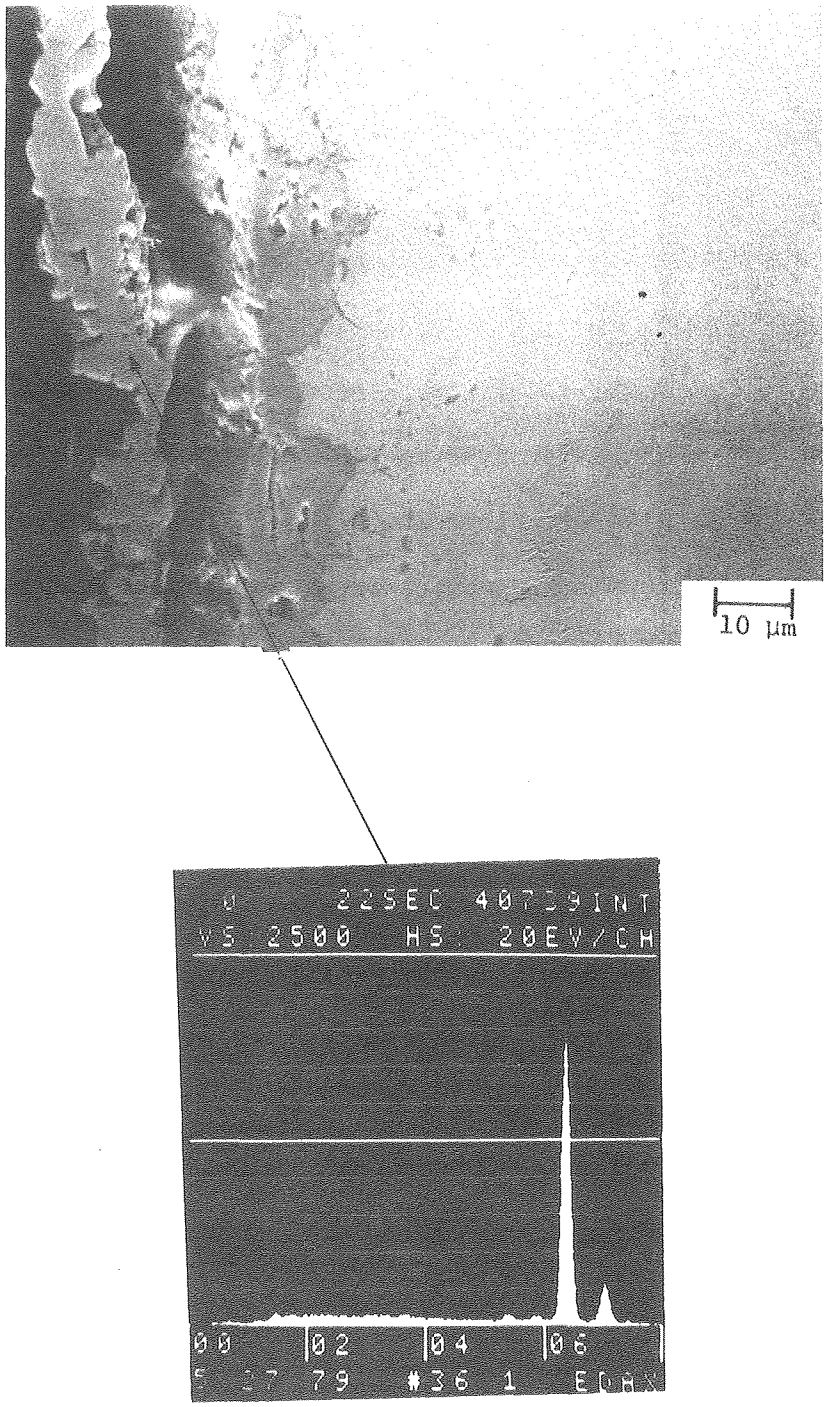

XBB 759-7480

Figure 28. Cross Section of a Sample Exposed to Graphite for 24 hours in Mixture B

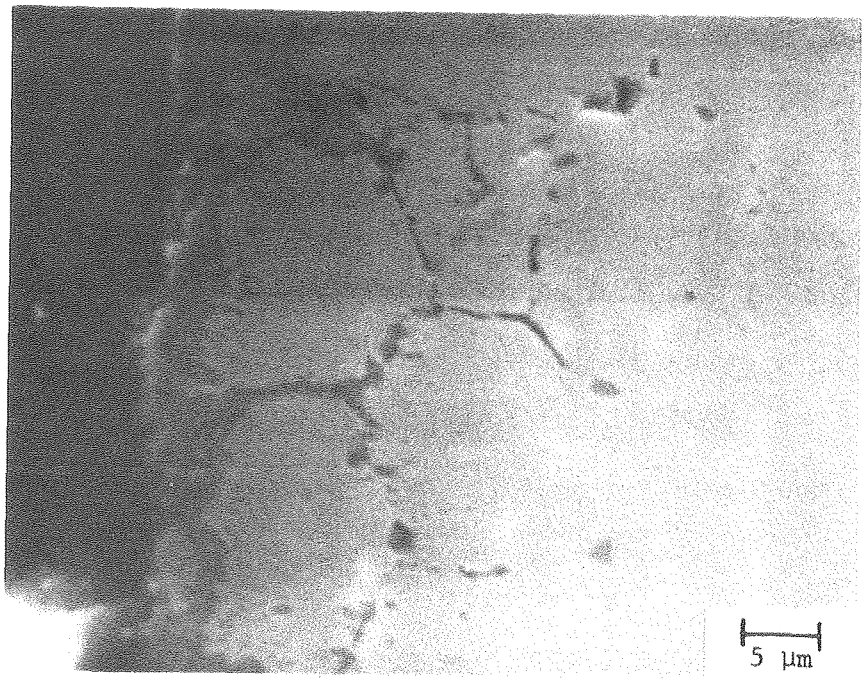

XBB 795-6902

Figure 29. Cross Section of a Sample Exposed to 0.5 gram Synthane Char in Mixture A for 24 hours

Since Synthane char contains excess calcium oxide which can react with the hydrogen sulfide in the gas to reduce the sulfur partial pressure to the one corresponding to the calcium oxide/calcium sulfide equilibrium, the sample again does not "see" the bulk gas.

In graphite, which does not contain calcium oxide or any other inorganic oxides, such reactions can not occur and the sulfur partial pressure at the metal surface is determined by the mass transfer through the graphite, not the calcium oxide/calcium sulfide equilibrium. If the bulk gas has a high sulfur content (mixture A) the sulfur partial pressure at the metal surface is high enough to cause sulfide scale formation. In the bulk gas which contains very little hydrogen sulfide (mixture B), the flux through the graphite is less and the sulfur partial pressure at the metal surface is much lower than in the former case. In this case sulfides are thermodynamically unstable at the metal surface.

CHAPTER 4: DISCUSSION

These experiments show that char significantly affects the corrosion of 304 stainless steel. The corrosion of other alloys will also be affected by the presence of coal char.

A. Effect of Coal Char on the Oxygen Partial Pressure

The carbon in char fixes the oxygen partial pressure at a value determined by the carbon/carbon monoxide equilibrium ($p_{O_2} < 10^{-18}$ atm). Many of today's alloys are designed to form protective oxide scales in combustion atmospheres which are much more oxidizing. The formation of protective oxide scales at the low oxygen partial pressures in coal char is much slower and more difficult than in combustion atmospheres. Under same conditions the metal sulfide may actually become thermodynamically more stable than the oxide because of the low oxygen partial pressure.

B. Patterns of Sulfidation in the Presence of Coal Char

Two patterns of sulfidation are described in Chapter 2. If the char reacts only with the carbon containing gaseous species, but not with the sulfur containing species, the layer of char acts as a resistance to the diffusion of hydrogen sulfide from the bulk gas through the char to the metal surface. If scales form on the metal surface, in many cases the rate of scale growth is controlled by the diffusion of hydrogen sulfide through the char, and not the diffusion of metal cations through the scale. The mass-transfer limit, the largest possible flux of hydrogen sulfide through the char, is inversely proportional to the thickness of the char layer and roughly directly proportional to the hydrogen sulfide concentration in the bulk gas. The equilibrium sulfur partial pressure at the metal surface differs

significantly from the sulfur partial pressure in the bulk gas only for hydrogen sulfide fluxes greater than 80% of the mass-transfer limit. Therefore, the steady state flux, the flux at which the hydrogen sulfide flux through the char and the metal cation flux through the scale are equal, is greater than 80% of the mass-transfer limit.

If the rate of sulfidation is controlled by the flux of hydrogen sulfide through the char, linear kinetics for the rate of scale growth will be observed. When the scale becomes thick enough, the rate of scale growth will be determined by the diffusion of metal cations through the scale, and the thickness of the scale will increase according to parabolic kinetics.

A similar switch from linear kinetics to parabolic kinetics is observed in the corrosion of alloys exposed to complex gases. Initially the weight gain is controlled by the diffusion of the reactive gases through the gaseous diffusion layer at the metal surface, and the weight gain is linear in time. When the scale is thick, outward cation diffusion limits the weight gain, and parabolic kinetics are observed.

If the char contains ash, i.e. inorganic sulfides and oxides, which will react with the sulfur containing species in the char or in the gas, the rate and pattern of sulfidation will be controlled by the thermodynamics of the reactions between the ash and the gas phase. For example, if the ash contains calcium oxide and calcium sulfide, the sulfur partial pressure of gas in contact with the char is determined by the calcium oxide/calcium sulfide equilibrium. The calcium oxide close to the bulk gas will be sulfidized to calcium sulfide. The calcium sulfide near the char-metal interface will be

oxidized. As long as the char has not been depleted of calcium oxide, the sulfur pressure of the gas in the char will be fixed by the calcium oxide/calcium sulfide equilibrium and independent of the composition and flow rate of the bulk gas, since the char effectively shields the alloy. Once all of the calcium oxide has reacted, the pattern of sulfidation will be similar to the one described for char which does not react with the sulfur containing gaseous species. The length of this initial transient period is proportional to the square of the char thickness. It is inversely proportional to the hydrogen sulfide concentration of the bulk gas.

A third pattern of attack occurs, if the char contains a lot of sulfur containing volatiles. If these are driven off, the sulfur pressure in the char depends on the quantity and composition of the volatiles. Only a finite amount of volatiles is in the char, therefore the extent of corrosion will decrease as the flow rate of the bulk gas over the char increases, since more of the volatiles are swept away by the bulk gas. Once all of the volatiles have been driven off, sulfidation similar to the corrosion in ash-free char will be observed.

C. Effect of Char Composition on the Pattern of Sulfidation

The patterns of attack discussed above are observed experimentally. The extensive attack observed on samples exposed to FMC char is due to devolitalization. Analysis of the FMC char and ash compositions indicates that the volatiles contain most of the sulfur in FMC char.

The FMC char used in these expeirments was formed in stage 2 of the FMC process, which is the coal liquefaction part of the process. The process diagram indicates that the char was not heated above 725 K during processing. Therefore volatiles will be driven off during these

experiments, since they are carried out at 1200 K. The most extensive attack is observed in closed environments since none of the volatiles leave the system. With gas flow in and out of the system some of the volatiles leave the system, which leads to a decrease in the extent of sulfidation. Presumably the volatiles produced are so rich in sulfur that the sulfur partial pressure in the char is independent of the composition of the bulk gas.

The corrosion of samples exposed to Husky and Synthane char is determined by the thermodynamics of the char-gas reactions. Since these chars contain considerable amounts of excess calcium oxide, the sulfur partial pressure in these chars is determined by the calcium oxide/calcium sulfide equilibrium. This equilibrium partial pressure is low enough to prevent the formation of sulfide scales. Instead only small internal sulfides are formed. As predicted, the extent of corrosion observed in short exposure times does not depend strongly on the covering gas composition or flow rate. In sulfur containing bulk gases the calcium oxide in the char reacts with hydrogen sulfide preventing its diffusion to the metal surface. In sulfur free bulk gases the calcium sulfide is oxidized to form hydrogen sulfide, which then reacts with the metal. Since the oxygen partial pressure is approximately the same in both cases, the sulfur pressure will be approximately the same also.

Mass-transfer effects are observed in the corrosion of samples in graphite and sulfur containing bulk gases. Since graphite is essentially pure carbon, it does not react with hydrogen sulfide in the gas phase, but instead acts as a mass-transfer resistance through which the hydrogen sulfide diffuses to the metal surface. As predicted, the rate of

sulfidation decreases as the depth of the char layer increases. In mixture A (1% H_2S) the sulfur pressure at the metal surface is large enough to cause external scale formation, not just internal sulfidation. In mixture B (0.01% H_2S) only internal sulfidation occurs.

Several interesting aspects about the effect of char should be emphasized. One is that chars like Synthane and Husky char, which contain excess calcium oxide (or other species which will react with sulfur, like magnesium for example), cause slower rates of sulfidation than chars which do not contain excess calcium oxide (graphite, for example). This reduction in the rate of sulfidation lasts only as long as all of the calcium oxide in the ash has not reacted. The experiments with graphite show that once the char is depleted of excess calicum oxide, external sulfide scales will form on the samples if the bulk gas contains enough hydrogen sulfide.

Thus, the sulfidation of samples exposed to chars containing excess calcium oxide consists of three periods. During the initial period when the composition of the gas in the char is controlled by the thermodynamics of the char-gas reactions, the sulfur partial pressure of the gas phase is very low, and only slight internal sulfidation occurs. However, because of the low oxygen partial pressure of the gas phase in the char, protective oxide scales do not form during this period. This initial period is followed by a period of linear kinetics. External sulfide scales will form, if the bulk gas contains enough hydrogen sulfide. During this time the rate of sulfidation is limited by the diffusion of hydrogen sulfide through the char. During this period the weight gain is linear with time. If a sulfide scale is formed, and hydrogen sulfide cannot diffuse

through the scale along grain boundaries, cracks, or voids caused by embedded char particles, the rate of scale growth will ultimately be controlled by the diffusion of metal cations through the scale and the rate of scale growth will follow parabolic kinetics.

D. Effect of Calcium Oxide

Alloys designed to form protective oxide scales to prevent sulfidation of the bulk metal will fail at the high temperatures planned for the new coal gasification processes, because the low oxygen partial pressure prevents the formation of protective oxide scales. Therefore ceramic linings and coatings will be necessary to protect the gasifier internals against sulfidation, unless radically new alloys which will form protective oxide scales at the oxygen partial pressures encountered in gasifiers are developed.

In the above discussion, the importance of calcium oxide in reducing the sulfur partial pressure was emphasized. It might be beneficial to feed calcium oxide at the top of the reactor mixed with the coal or separately. This would reduce the sulfur partial pressure of the gas in the gasifier, making it less sulfidizing. It might be possible to remove enough hydrogen sulfide from the gas to eliminate the need to scrub the gas leaving the gasifier. The calcium sulfide formed and unreacted calcium oxide would leave the reactor with the char. The calcium oxide would be recovered by burning the char completely in a separate reactor.

The CO_2 Acceptor process, shown in Figure 30, is similar to the process described above. Dolomite, a mixture of calcium oxide and magnesium oxide, is used. Dolomite reacts with carbon dioxide to form calcium carbonate and magnesium carbonate. This exothermic reaction

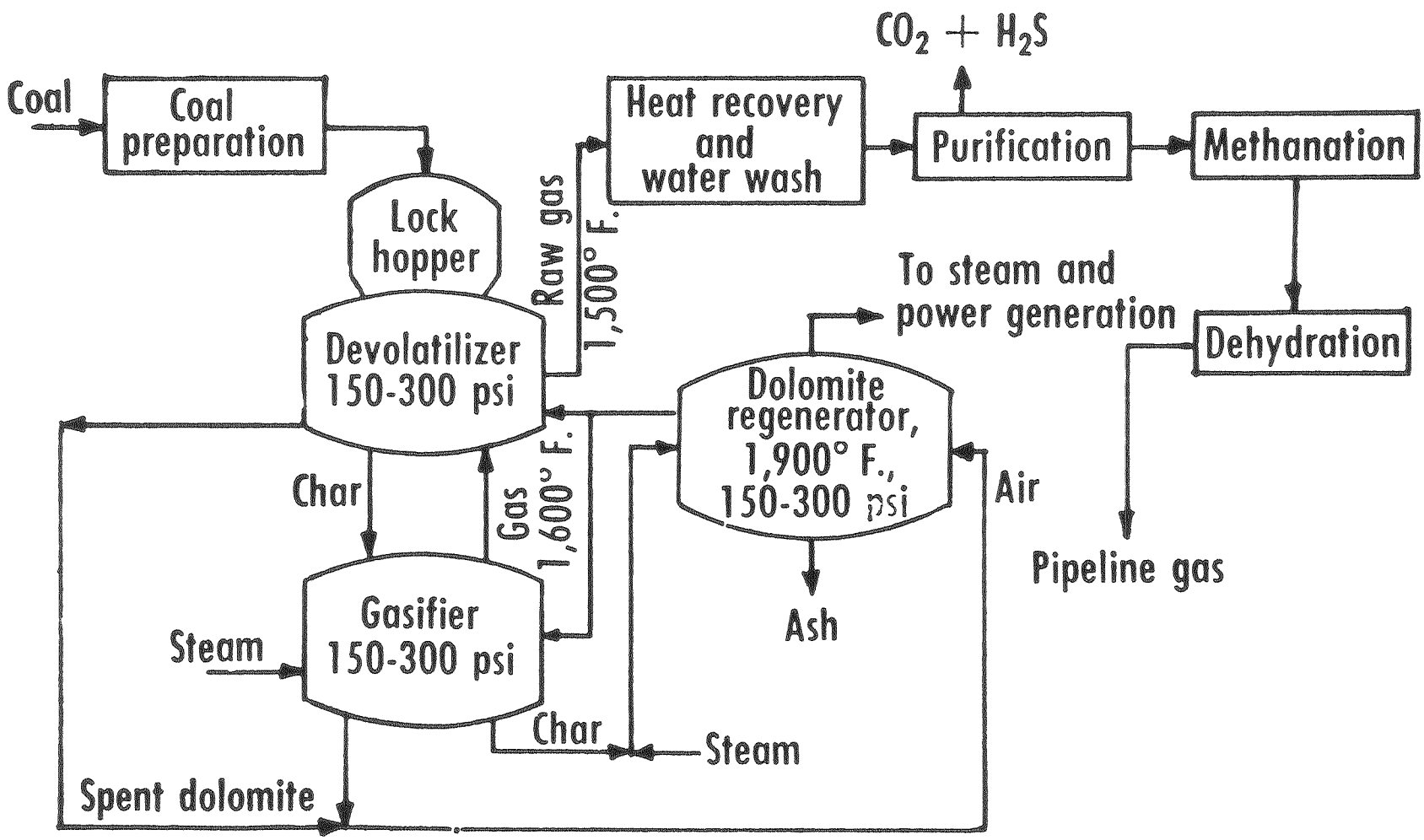

Figure 30. Process Diagram for the CO_2-Acceptor Coal Gasification Process (from Ref. 3)

produces the heat for the endothermic methanation and carbon-water reactions. The calcined Dolomite is regenerated by burning it and the residual char in a separate furnace. Possibly a similar, though smaller loop, can be incorporated into the other designs, not to supply heat but to remove hydrogen sulfide from the gas phase.

E. Summary

Below the effects of coal char on sulfidation discussed above are summarized briefly.

1. Since coal char contains a large amount of carbon, the oxygen partial pressure at the metal surface is less than 10^{-18} atm which prevents the formation of protective oxide scales. In some cases the sulfide may be thermodynamically more stable than the oxide.

2. The effect of coal char on the sulfidation of alloys depends on the composition of the char. Very extensive sulfidation occurs in the presence of chars which contain significant amounts of sulfur rich volatiles (FMC char, for example). Very little sulfidation occurs in samples exposed to chars containing excess calcium oxide. These chars include Synthane and Husky char. Mass-transfer effects are observed with chars which do not interact with the sulfur containing gaseous species (graphite, for example). In this case the extent of sulfidation is inversely proportional to the thickness of the char layer, and roughly directly proportional to the hydrogen sulfide concentration of the bulk gas.

3. The presence of calcium oxide significantly reduces the sulfur partial pressure of the gas phase in contact with the char. At the low oxygen partial pressures in coal gasifiers, the calcium oxide/calcium sulfide equilibrium fixes the sulfur partial pressure at a value below

10^{-11} atm. This reduces the rate and extent of sulfidation.

F. Recommendations for Future Work

The above discussion shows that further experiments are necessary to complete our understanding of the effect of coal char on corrosion. Long term tests with Synthane char and others, if they are available, in sulfur-containing gases should be carried out to test if the predicted switch from minor internal sulfidation to external scale formation occurs. Experiments at 1200 K with FMC char obtained from the second stage of the FMC process should not be continued, since the char is only heated to 725 K (850°F) during the first two stages of the process. At those temperatures the char has not been completely devolitalized. Therefore, it is unrealistic to run experiments with FMC char at 1200 K, where it will be devolatilized completely.

The effect of calcium oxide on the sulfur partial pressure should also be investigated more fully. Samples could be exposed to synthetic chars consisting of graphite and calcium oxide, and other inorganic sulfides or sulfates such as calcium sulfide, calcium sulfate, iron sulfide, etc. The presence of graphite or some other carbon containing compound is crucial to ensure the low oxygen partial pressure which inhibits the formation of protective oxide scales.

Some of the experiments with small amounts of char indicate that the kinetics of the reactions between the char and the carbon dioxide and oxygen are not as fast as assumed in developing the model. The kinetics of the char-gas reactions could be studied by passing gases through packed beds of char heated to 1200 K and measuring the composition of the exit gas. These compositions could be used to fit kinetic parameters for char-gas reactions.

ACKNOWLEDGMENT

I want to thank Professor John Newman, Professor David Whittle, and Alan Levy for their support and guidance during this project. Their suggestions and comments, which helped to clarify many concepts and ideas, were an invaluable aid.

I am also very grateful to Glenn Baum for his patient help in implementing modifications of the experimental apparatus. I am especially grateful to Carol Payne, who always knew of whom to go to and how to get things done. Finally, I want to thank Nancy Charpentier for typing this manuscript on such short notice.

This work was performed under a grant from the United States Department of Energy Division of Basic Energy Sciences.

APPENDIX

Printouts of the computer programs used to calculate the concentration profiles are presented below. The arrays are dimensioned for a maximum of eight gaseous species, five char-gas reactions, and two reactions at the char-metal interface. The maximum number of nodes is eleven.

CHAR (INPUT, OUTPUT)

The main program, CHAR, reads the input data and then calls COMPOS. The variables are listed below.

C	mole fractions
CF	stoichiometric coefficients for hydrogen balance
DIFF	effective binary diffusion coefficient
EQUIL	equilibrium constants for the reactions in the char
EQUILS	equilibrium constants for the reactions at the char-metal interface
FLUX	N_i
GNU	stoichiometric coefficients for reactions in the char
H	step size
LIM	maximum number of iteration for convergence
N	number of species
NAME	name of species
NJ	number of nodes
NR	number of reactions in char
NRS	number of reactions at char-metal interface
RATE	rate constants for reactions in char
RATES	rate constants for reactions at char-metal interface

S	exponents for the rate expressions of the char-metal reactions
SM	stoichiometric coefficients of the gaseous species of the char-metal reactions
XX	initial estimate of mole fractions

```
      PROGRAM CHAR(INPUT,OUTPUT)
      COMMON/M/CF(8),FLUX(8,11),DIF(8,8),XX(8,11),NR,GNU(8,5),RATE(5)
     1,EQUIL(5),NRS,S(8,2),SM(8,2),RATES(2),EQUILS(2),NJ
      DIMENSION NAME(8)
1     FORMAT(3I10,E10.0)
2     FORMAT(8A10)
3     FORMAT(8E10.0)
4     FORMAT(2E10.0,8E5.0)
5     FORMAT(8E5.0)
11    FORMAT(*1PROBLEM STATEMENT*//* N=*,I4/* LIM=*,I4/* NJ=*,I4/* H=*,F
     17.4)
12    FORMAT(/* DIFFUSION COEFFICIENTS*/11X,7A10)
13    FORMAT(* *,A10,7E12.5)
14    FORMAT(/* INITIAL CONDS*,8E12.5)
15    FORMAT(/* NR=*,I4/* L,RATE(L),EQUIL(L),GNU(N,L)*)
16    FORMAT(* *I5,2X,2E10.5,8F8.3)
17    FORMAT(/* NRS=*,I4/* L,RATES(L),EQUILS(L),S(K,L)*)
18    FORMAT(* SM(K,L)*,5X,I5,2X,8F8.3)
      READ 1,N,LIM,NJ,H
      READ 2,(NAME(K),K=1,N)
      NM1=N-1 $ DO 100 K=1,NM1
      KK=K+1
      READ 3,(DIF(K,J),J=KK,N)
      DO 100 J=KK,N
100   DIF(J,K)=DIF(K,J)
      READ 3,(XX(K,NJ),K=1,N)
      READ 3,(CF(K),K=1,N)
      READ 1,NR,NRS
      DO 200 L=1,NR
      READ 4, RATE(L),EQUIL(L),(GNU(K,L),K=1,N)
      RATE(L)=RATE(L)/100.
200   EQUIL(L)=EXP(-EQUIL(L))
      DO 300 L=1,NRS
300   READ 4,RATES(L),EQUILS(L),(S(K,L),K=1,N)
      DO 400 L=1,NRS
400   READ 5,(SM(K,L),K=1,N)
      NJM1=NJ-1
      DO 500 J=1,NJM1 $ DO 500 K=1,N
500   XX(K,J)=XX(K,NJ)
      PRINT 11,N,LIM,NJ,H
      PRINT 12,(NAME(K),K=1,NM1)
      DO 1100 KK=2,N
      KM=KK-1
1100  PRINT 13,NAME(KK),(DIF(KK,K),K=1,KM)
      PRINT 14,(XX(K,NJ),K=1,N)
      PRINT 15,NR
      DO 1200 L=1,NR
1200  PRINT 16,L,RATE(L),EQUIL(L),(GNU(K,L),K=1,N)
      PRINT 17,NRS
      DO 1300 L=1,NRS
1300  PRINT 16,L,RATES(L),EQUILS(L),(S(K,L),K=1,N)
      DO 1400 L=1,NRS
1400  PRINT 13,L,(SM(K,L),K=1,N)
      CALL COMPOS(N,LIM,H)
      STOP $ END
```

COMPOS (N, LIM, H)

For each J, COMPOS first calls MATINV to invert the Stefan-Maxwell equations and Equation 2. The coefficients of the finite difference approximations of Equations 4, 9, 10, 11 and 12 are then calculated. These equations have the following form

$$\sum_{k} \left\{ A(I,K) \cdot C(K,J-1) + B(I,K) \cdot C(K,J) + D(I,K) \cdot (C,J+1) \right\} = G(I)$$

for I=1, N

After A, B, D, and G have been determined, control is transferred to BAND. This program is discussed in more detail in Reference 14.

```
      SUBROUTINE COMPOS(N,LIM,H)
      COMMON/M/CF(8),FLUX(8,11),DIF(8,8),XX(8,11),NR,GNU(8,5),RATE(5)
     1,EQUIL(5),NRS,S(8,2),SM(8,2),RATES(2),EQUILS(2),NJJ
      COMMON A(8,8),B(8,8),C(8,11),D(8,17),G(8),X(8,8),Y(8,8),NN,NJ
      DIMENSION DX(8),S1(8),S2(8),S3(8,8),BINV(8,8),S4(8),S5(8)
      NN=N  $ NJ=NJJ
      DO 1 J=1,NJ  $  DO 1 I=1,N
    1 C(I,J)=XX(I,J)
      ITERAT=0
    8 J=0 $ ITERAT=ITERAT+1 $ DO 9 I=1,N $ DO 9 K=1,N $ X(I,K)=0.0
    9 Y(I,K)=0.0
   10 J=J+1 $ DO 11 I=1,N $ G(I)=0.0 $ D(I,N+1)=0.0 $ XX(I,J)=C(I,J)
      DO 11 K=1,N $ A(I,K)=0.0 $ B(I,K)=0.0 $ S3(I,K)=0.0
   11 D(I,K)=0.0 $ IF(J.NE.1) GO TO 13 $ G(1)=1.0  $ DO 12 I=2,N
      D(I,I)=-2.0/H $ X(I,I)=0.5/H $ B(I,I)=1.5/H
   12 B(1,I)=1.0 $ B(1,1)=1.0
C     HETEROGENEOUS REACTIONS
      IF(NRS.EQ.0) GO TO 49 $ DO 48 L=1,NRS $ RLB=RATES(L)
      RLF=RLB*EQUILS(L) $ DO 43 I=1,N $ IF(S(I,L))  39,43,41
   39 IF(C(I,1).GT.0.0) GO TO 40 $ RLB=0.0 $ GO TO 43
   40 RLB=RLB*C(I,1)**(-S(I,L)) $ GO TO 43
   41 IF(C(I,1).GT.0.0) GO TO 42 $ RLF=0.0 $ GO TO 43
   42 RLF=RLF*C(I,1)**S(I,L)
   43 CONTINUE
      DO 48 I=2,N $ DO 48 K=1,N $ IF(K.EQ.I) GO TO 48
      B(I,I)=B(I,I)-SM(K,L)*(RLF-RLB)/DIF(I,K)
      B(I,K)=B(I,K)+SM(I,L)*(RLF-RLB)/DIF(I,K)
      SAV=-(C(I,1)*SM(K,L)-C(K,1)*SM(I,L))/DIF(I,K) $ DO 47 JJ=1,N
      IF(C(JJ,1).LE.0.0) GO TO 47 $ IF(S(JJ,L))  44,47,45
   44 SAVE=SAV*RLB*S(JJ,L)/C(JJ,1) $ GO TO 46
   45 SAVE=SAV*RLF*S(JJ,L)/C(JJ,1)
   46 B(I,JJ)=B(I,JJ)+SAVE $ G(I)=G(I)+SAVE*C(JJ,1)
   47 CONTINUE
   48 CONTINUE
   49 CONTINUE
      CALL BAND(J) $ GO TO 10
   13 IF(J.EQ.NJ) GO TO 16 $            DO 14 K=1,N $ B(1,K)=CF(K)
      S4(K)=0.0 $ S5(K)=0.0
      D(K,K)=1.0 $ DX(K)=C(K,J+1)-C(K,J-1)
      IF(K.EQ.1) GO TO 14 $ DO 18 I=1,N $ IF(I.EQ.K) GO TO 18
      B(K,I)=C(K,J)/DIF(I,K)   $ B(K,K)=B(K,K)-C(I,J)/DIF(I,K)
   18 CONTINUE $ D(K,N+1)=DX(K)/2.0/H
   14 CONTINUE $ CALL MATINV(N,N+1,DETERM) $ DO 20 I=1,N
      FLUX(I,J)=D(I,N+1) $ DO 19 K=1,N $ BINV(I,K)=D(I,K) $ B(I,K)=0.0
   19 D(I,K)=0.0
   20 B(1,I)=1.0 $ DO 22 I=1,N $ S1(I)=0.0 $ S2(I)=0.0 $ DO 22 K=1,N
      IF(K.EQ.I) GO TO 22 $ A2=FLUX(K,J)/DIF(I,K)
      S4(I)=S4(I)+FLUX(K,J)/DIF(I,K)
      S5(I)=S5(I)+FLUX(K,J)/DIF(I,K)
      A1=(C(K,J+1)/DIF(I,K)     -C(K,J-1)/DIF(I,K)     )/2.0/H
      S1(I)=S1(I)+A1 $ S2(I)=S2(I)+A2 $ DO 21 L=1,N
   21 S3(L,K)=S3(L,K)+BINV(I,L)*A1
   22 CONTINUE
      DO 15 I=2,N $ G(I)=G(I)-FLUX(I,J)*S1(I)
      S4(I)=S4(I)/2.0/H $ S5(I)=S5(I)/2.0/H
      DO 27 K=1,N $ S3(K,I)=S3(K,I)-BINV(I,K)*S1(I)
```

```
      IF(K.NE.1) D(I,K)=S3(K,I)+D(I,K) $ IF(K.EQ.I) GO TO 27
   27 CONTINUE $ DO 24 K=1,N
      D(I,K)=D(I,K)/2.0/H $ A(I,K)=-D(I,K) $ DO 23 L=2,N
   23 IF(L.NE.K) B(I,K)=B(I,K)+FLUX(L,J)/DIF(K,L)  *S3(L,I)
      IF(K.NE.1) B(I,K)=B(I,K)-S2(K)*S3(K,I)
      IF(K.EQ.I) GO TO 24
      G(I)=G(I)+B(I,K)*C(K,J)
      D(I,K)=D(I,K)-FLUX(I,J)/DIF(I,K     )/2.0/H
      A(I,K)=A(I,K)+FLUX(I,J)/DIF(I,K     )/2.0/H
   24 CONTINUE          $ D(I,I)=D(I,I)+S4(I)-1.0/H/H
      A(I,I)=A(I,I)-S5(I)-1.0/H/H
      G(I)=G(I)+B(I,I)*C(I,J)+S4(I)*C(I,J+1)-S5(I)*C(I,J-1)
   15 B(I,I)=B(I,I)+2.0/H/H
C     HOMOGENEOUS CHEMICAL REACTIONS
      IF(NR.EQ.0) GO TO 38 $ DO 37 L=1,NR $ RJB=RATE(L)
      RJF=RJB*EQUIL(L)    $ DO 32 I=1,N $ IF(GNU(I,L)) 28,32,30
   28 IF(C(I,J).GT.0.0) GO TO 29 $ RJB=0.0 $ GO TO 32
   29 RJB=RJB*C(I,J)**(-GNU(I,L)) $ GO TO 32
   30 IF(C(I,J).GT.0.0) GO TO 31 $ RJF=0.0 $ GO TO 32
   31 RJF=RJF*C(I,J)**GNU(I,L)
   32 CONTINUE
                 DO 37 I=2,N $ DO 37 K=1,N $ IF(K.EQ.I) GO TO 37
      B(I,I)=B(I,I)-GNU(K,L)*(RJF-RJB)/DIF(I,K)
      B(I,K)=B(I,K)+GNU(I,L)*(RJF-RJB)/DIF(I,K)
      SAV=-(C(I,J)*GNU(K,L)-C(K,J)*GNU(I,L))/DIF(I,K)    $ DO 36 JJ=1,N
      IF(C(JJ,J).LE.0.0) GO TO 36 $ IF(GNU(JJ,L))  33,36,34
   33 SAVE=SAV*RJB*GNU(JJ,L)/C(JJ,J) $ GO TO 35
   34 SAVE=SAV*RJF*GNU(JJ,L)/C(JJ,J)
   35 B(I,JJ)=B(I,JJ)+SAVE $ G(I)=G(I)+SAVE* C(JJ,J)
   36 CONTINUE
   37 CONTINUE
   38 CONTINUE
      G(1)=1.0 $ CALL BAND(J) $ GO TO 10
   16 DO 17 I=1,N  $  B(I,I)=1.0
   17 G(I)=C(I,NJ)
      CALL BAND(J)
      PRINT 101,ITERAT $ ID=0 $ DO 51 J=1,NJ
      PRINT 102,J,(C(K,J),K=1,N) $ DO 51 K=1,N
      IF(C(K,J).LT.XX(K,J)/100.)C(K,J)=XX(K,J)/100.
51    IF(ABS(XX(K,J)-C(K,J)).GE.1.E-6*C(K,J))IC=1
      DO 52 J=1,NJ
52    PRINT 102,J,(FLUX(K,J),K=1,N)
      IF(ID.EQ.1.AND.ITERAT.LT.LIM)GOTO 8
      XS2=.04328*C(5,1)/C(6,1)  $  XS2=XS2*XS2
      XO2=6.338E-18*C(2,1)
      PRINT 104,XS2,XO2
      IF(ID.EQ.0)RETURN
      PRINT 103,LIM
101   FORMAT(*1ITERATION*,I4)
102   FORMAT(* *,I4,8E13.6)
103   FORMAT(*1THE PROGRAM DID NOT CONVERGE IN *,I2,*ITERATIONS*)
104   FORMAT(///* CONDITIONS AT Z=0,  XS2=*,E13.6,*XO2 =*,E13.6)
      STOP $ END
```

BAND (J) and MATINV (N,M,DETERM)

BAND is called for each value of J, for J=1, NJ. During the first pass calculated intermediate values are stored in E. After the calculations for J = NJ are complete, the program automatically uses the values stored in E to calculate C.

MATINV is called by both COMPOS and BAND to invert matrices. Both of these programs are described in detail in References 20 and 21.

```
      SUBROUTINE BAND(J)
      DIMENSION A(8,8),B(8,8),C(8,11),D(8,17),G(8),E(8,9,11),X(8,8)
      DIMENSION Y(8,8)
      COMMON A,B,C,D,G,X,Y,N,NJ
  101 FORMAT (15H0DETERM=0 AT J=,I4)
      IF (J-2)  1,6,8
    1 NP1= N + 1
      DO 2 I=1,N
      D(I,2*N+1)= G(I)
      DO 2 L=1,N
      LPN= L + N
    2 D(I,LPN)= X(I,L)
      CALL MATINV (N,2*N+1,DETERM)
      IF (DETERM)  4,3,4
    3 PRINT 101,J
    4 DO 5 K=1,N
      E(K,NP1,1)= D(K,2*N+1)
      DO 5 L=1,N
      E(K,L,1)= - D(K,L)
      LPN= L + N
    5 X(K,L)= - D(K,LPN)
      RETURN
    6 DO 7 I=1,N
      DO 7 K=1,N
      DO 7 L=1,N
    7 D(I,K)= D(I,K) + A(I,L)*X(L,K)
    8 IF (J-NJ)  11,9,9
    9 DO 10 I=1,N
      DO 10 L=1,N
      G(I)= G(I) - Y(I,L)*E(L,NP1,J-2)
      DO 10 M=1,N
   10 A(I,L)= A(I,L) + Y(I,M)*E(M,L,J-2)
   11 DO 12 I=1,N
      D(I,NP1)= - G(I)
      DO 12 L=1,N
      D(I,NP1)= D(I,NP1) + A(I,L)*E(L,NP1,J-1)
      DO 12 K=1,N
   12 B(I,K)= B(I,K) + A(I,L)*E(L,K,J-1)
      CALL MATINV (N,NP1  ,DETERM)
      IF (DETERM)  14,13,14
   13 PRINT 101,J
   14 DO 15 K=1,N
      DO 15 M=1,NP1
   15 E(K,M,J)= - D(K,M)
      IF (J-NJ)  20,16,16
   16 DO 17 K=1,N
   17 C(K,J)= E(K,NP1,J)
      DO 18 JJ=2,NJ
      M= NJ - JJ + 1
      DO 18 K=1,N
      C(K,M)= E(K,NP1,M)
      DO 18 L=1,N
   18 C(K,M)= C(K,M) + E(K,L,M)*C(L,M+1)
      DO 19 L=1,N
      DO 19 K=1,N
   19 C(K,1)= C(K,1) + X(K,L)*C(L,3)
   20 RETURN
      END
```

```
      SUBROUTINE MATINV(N,M,DETERM)
      COMMON A(8,8),B(8,8),C(8,11),D(8,17)
      DIMENSION ID(8)
      DETERM=1.0 $ DO 1 I=1,N
    1 ID(I)=0 $ DO 18 NN=1,N $ BMAX=1.0 $ DO 6 I=1,N
      IF(ID(I).NE.0) GOTO 6 $ BNEXT=0.0 $ BTRY=0.0 $ DO 5 J=1,N
      IF(ID(J).NE.0) GOTO 5 $ IF(ABS(B(I,J)).LE.BNEXT) GOTO 5
      BNEXT=ABS(B(I,J)) $ IF(BNEXT.LE.BTRY) GOTO 5 $ BNEXT=BTRY
      BTRY=ABS(B(I,J)) $ JC=J
    5 CONTINUE $ IF(BNEXT.GE.BMAX*BTRY) GOTO 6
      BMAX=BNEXT/BTRY $ IROW=I $ JCOL=JC
    6 CONTINUE $ IF(ID(JC).EQ.0) GOTO 8 $ DETERM=0.0 $ RETURN
    8 ID(JCOL)=1 $ IF(JCOL.EQ.IROW) GOTO 12 $ DO 10 J=1,N
      SAVE=B(IROW,J) $ B(IROW,J)=B(JCOL,J)
   10 B(JCOL,J)=SAVE $ DO 11 K=1,M $ SAVE=D(IROW,K)
      D(IROW,K)=D(JCOL,K)
   11 D(JCOL,K)=SAVE
   12 F=1.0/B(JCOL,JCOL) $ DO 13 J=1,N
   13 B(JCOL,J)=B(JCOL,J)*F $ DO 14 K=1,M
   14 D(JCOL,K)=D(JCOL,K)*F $ DO 18 I=1,N $ IF(I.EQ.JCOL) GO TO 18
      F=B(I,JCOL) $ DO 16 J=1,N
   16 B(I,J)=B(I,J)-F*B(JCOL,J) $ DO 17 K=1,M
   17 D(I,K)=D(I,K)-F*D(JCOL,K)
   18 CONTINUE $ RETURN $ END
```

Symbols

b_{ik}	coefficients of inverted Stefan-Maxwell equations
c	mol gas per unit volume (mol cm^{-3})
c_o	initial concentration of calcium oxide in char (mol cm^{-3})
c_s	initial concentration of calcium sulfide in char (mol cm^{-3})
(ΔC_p)	difference between the heat capacity of the products and the reactants
D_{ij}	effective binary diffusion coefficient of the pair i-j in a porous medium (cm^2 s^{-1})
$\mathcal{D}_{ij}$	binary diffusion coefficient for the pair i-j (cm^2 s^{-1})
k	Boltzman constant
K_j	equilibrium constant for reaction j
k_p	parabolic rate constant for scale growth (g^2 cm^{-4} s^{-1})
k_p'	k_p M_S^{-2}, parabolic rate constant for scale growth (mol^2 cm^{-4} s^{-1})
k_{jb}	rate constant for backward reaction
k_{jf}	rate constant for forward reaction
L	thickness of char layer (cm)
L_G	penetration of sulfidized calcium oxide from the char-gas interface (cm)
L_M	penetration of the oxidized calcium sulfide from the char-metal interface (cm)
M_A	molecular weight of species A
n	exponent for dependence of D_{ij} on ε
N_i	flux of species i relative to stationary coordinates (mol cm^{-2} s^{-1})
$\mathcal{N}_i$	$N_i \cdot L$ (mol cm^{-1} s^{-1})

N_i^o	initial estimate of N_i (mol cm^{-1} s^{-1})
p_i	partial pressure of species i (atm)
R	gas constant
R_i	rate of formation of species i (mol cm^{-3} s^{-1})
$\mathcal{R}_i$	$R_i \cdot L^2$ (mol cm^{-1} s^{-1})
r_{jb}	rate of backward reaction (mol cm^{-3} s^{-1})
r_{jf}	rate of forward reaction (mol cm^{-3} s^{-1})
t	time (s)
T	temperature (K)
T_b	normal boiling point (K)
V_b	molar volume at normal boiling point (mol cm^{-3})
(ΔW)	weight gain (g)
x_i	mole fraction of species i
x_i^o	initial estimate of x_i
z	distance from char-metal interface (cm)
ε_{AB}	energy of interaction for Lenard-Jones model
ε	void fraction of char
$\Omega_{\mathcal{D}}$	collision integral for diffusion coefficients
σ	Lenard-Jones radius
$\nu_{i,k}$	stoichiometric coefficient of element k in species i
ζ	$\frac{z}{L}$, dimensionless distance from char-metal interface

REFERENCES

1. Perry, Harry, "Coal Conversion Technology". Chemical Engineering, July 22, 1974, pp. 88-102.
2. Schora, Frank, "Clean Energy from Coal". 9th Intersociety Energy Conversion Engineering Conference.
3. Bodle, William and Vyos, Kirit, "Clean Fuels from Coal". The Oil and Gas Journal, August 26, 1974, pp. 73-88.
4. Nateson, K. and Chopra, O. K., "Corrosion Behavior of Materials for Coal Gasification Applications". Symposium on Properties of High Temperature Alloys. Las Vegas, Nevada, October 18-21, 1976.
5. Gordon, B. and Nagarajan, V., "Corrosion of Fe-10Al-Cr Alloys by Coal Char". LBL-6946, October 1977.
6. Birks, N., "Corrosion Mechanisms of Metals and Alloys in Multi-component Oxidative Environments". Symposium on Properties of High Temperature Alloys, Las Vegas, Nevada, October 18-21, 1976.
7. Gordon, B. and Nagarajan, V., "Preliminary Observations of the Thermodynamic Predictions of Fe-Cr-Ni Alloys in Coal Gasifier Environments". LBL-7606, March 1978.
8. Gulbransen, E., et al., "Thermodynamic Stability Diagrams for Condensed Phases in Selected Metal-Sulfur-Oxygen Systems Between 1150 K and 1450 K". University of Pittsburgh, November 1977.
9. Luthra, K. and Worrell, W., "Corrosion of Nickel in SO_2-O_2-SO_3 Atmospheres at 603°C". Symposium on Properties of High Temperature Alloys. Las Vegas, Nevada, October 18-21, 1976.

10. Private communication from Dave Whittle.

11. Gordon, B., "Corrosion of Iron-Base Alloys by Coal Char at 871°C and 982°C" (M.S. Thesis), LBL-7604, March 1978.

12. Douglass, D. and Bhide, V., "Mechanism of Corrosion of Structural Materials in Coal Gasifier Atmospheres". UCLA, February 1978.

13. Douglass, D., et al., "Mechanism of Corrosion of Structural Materials in Coal Gasifier Atmospheres". UCLA, August 1978.

14. Pollard, R. and Newman, J., "Silicon Deposition on a Rotating Disk", LBL-9154, to be published.

15. Sherwood, Thomas, Pigford, Robert, and Wilke, Charles, Mass Transfer. McGraw-Hill, 1975.

16. Bird, R., Stewart, W., and Lightfoot, E., Transport Phenomena. John Wiley & Sons, 1960.

17. Reid, Robert, Prausnitz, John, and Sherwood, Thomas, The Properties of Gases and Liquids. McGraw-Hill, 1977.

18. JANAF Thermochemical Tables. National Bureau of Standards, June 1971.

19. Elliott, John and Gleiser, Molly, Thermochemistry for Steelmaking. Addison-Wesley Publishing, 1960.

20. White, Ralph, et al., "The Fluid Motion Generated by a Rotating Disk: A Comparison of Solution Techniques". LBL-3910, November 1975.

21. Newman, John, Electrochemical Systems. Prentice Hall, 1973.

This report was done with support from the Department of Energy. Any conclusions or opinions expressed in this report represent solely those of the author(s) and not necessarily those of The Regents of the University of California, the Lawrence Berkeley Laboratory or the Department of Energy.

Reference to a company or product name does not imply approval or recommendation of the product by the University of California or the U.S. Department of Energy to the exclusion of others that may be suitable.

TECHNICAL INFORMATION DEPARTMENT
LAWRENCE BERKELEY LABORATORY
UNIVERSITY OF CALIFORNIA
BERKELEY, CALIFORNIA 94720